REPORT DOCUMENTATION PAGE

Form Approved OMB No. 0704-0188

1. AGENCY USE ONLY (*Leave Blank*)	2. REPORT DATE	3. REPORT TYPE AND DATES COVERED
	February, 1995	Final Report 29 April 94 - 28 Feb., 95

4. TITLE AND SUBTITLE

In-Situ Methods for Study of Fuel Thermal Stability

5. FUNDING NUMBERS

C-F33615-94-C-2434

6. AUTHOR(S)

Michael A. Serio, Erik Kroo, Anthony S. Bonanno, Kim S. Knight, Stuart Farquharson and Peter R. Solomon

7. PERFORMING ORGANIZATION NAME(S) AND ADDRESS(ES)

Advanced Fuel Research, Inc.
87 Church Street
PO Box 380379
East Hartford, CT 06138-0379

8. PERFORMING ORGANIZATION REPORT NUMBER

526031

9. SPONSORING/MONITORING AGENCY NAME(S) AND ADDRESS(ES)

USAF/AFMC/ASC
Wright Laboratory WL/POKA, Bldg 7
2530 C Street
Wright-Patterson AFB, OH 45433-7607

10. SPONSORING/MONITORING AGENCY REPORT NUMBER

11. SUPPLEMENTARY NOTES

12a. DISTRIBUTION/AVAILABILITY STATEMENT

DISTRIBUTION STATEMENT A
Approved for public release;
Distribution Unlimited

12b. DISTRIBUTION CODE

13. ABSTRACT (*Maximum 200 words*)

The objective of this work was to develop a methodology for in-situ optical measurements of peroxide decomposition products from aviation fuels and demonstrate how this information could be related to fuel stability. Three fiber optic probes (2 Mid-IR, 1 Near-IR) were designed and constructed, and used to monitor the changes in composition of two fuels (Shell Jet A #2827 and Sun Jet A-1 #2747) after thermal stressing. Both mid-IR probes were found to be very sensitive to changes in fuel composition. The large gap (1 mm) IR cell was used to make in-situ IR transmission measurements for peroxide decomposition products, including carbonyls (free and acid form), alcohols, and CO_2 (two forms). These measurements were consistent with the generally accepted free radical mechanism of fuel degradation, including the inverse relationship between oxidative and thermal stability. The data from the small gap (0.1 mm) IR cell were found to be consistent with changes in deposit formation tendencies with temperature for similar fuels reported in the literature. In an option task, an FT-Raman probe was evaluated and found to be much less sensitive than the Mid-IR probes. This disadvantage may be remedied by the use of a surface enhanced probe. The potential applications include an instrument for development and evaluation of thermally stable fuels or supercritical fuels, improved global models of fuel degradation mechanisms, and on-board monitors of fuel thermal stability.

14. SUBJECT TERMS	15. NUMBER OF PAGES
Thermal Stability, Aviation Fuels, FT-IR, FT-Raman, Diagnostics Fiber Optics	53
	16. PRICE CODE

17. SECURITY CLASSIFICATION OF REPORT	18. SECURITY CLASSIFICATION OF THIS PAGE	19. SECURITY CLASSIFICATION OF ABSTRACT	20. LIMITATION OF ABSTRACT
Unclassified	Unclassified	Unclassified	UL

WL-TR-94-

IN-SITU METHODS FOR STUDY OF FUEL THERMAL STABILITY

Michael A. Serio, Erik Kroo, Anthony S. Bonanno, Kim S. Knight, Stuart Farquharson, and Peter R. Solomon

ADVANCED FUEL RESEARCH, INC.
87 Church Street
East Hartford, CT 06108

February, 1995

Final Report for Period - 29 April 1994 - 28 February 1995

Approved for public release; distribution is unlimited.

Aero Propulsion and Power Directorate
Wright Laboratory
Air Force Materiel Command
Wright-Patterson AFB, OH 45433-7650

Table of Contents

Figure	List of Figures	Page

Figure	List of Figures "Continued"	Page

Table	List of Tables	Page

ACKNOWLEDGEMENTS

The authors gratefully acknowledge the support of this work by the U.S. Air Force under Contract No. F33615-94-C-2434. The authors also wish to thank the Project Officer, Lt. John Garver, for his help and support. Ms. Marie DiTaranto, of Advanced Fuel Research, Inc., assisted with the experimental work. The authors also wish to acknowledge helpful discussions with Prof. Eric Suuberg of Brown University. The preparation of the manuscript and figures was ably performed by Karin Keith and Lori Bellone.

2. EXECUTIVE SUMMARY

2.1. The Problem

The fuel is utilized as a primary heat sink on most aircraft. Consequently, the development of advanced high speed aircraft using hydrocarbon fuels will require fuels which have very high thermal stability, including fuels which can be stable above the critical temperature and pressure. In addition, the expected transition to fuels from new sources will require a more fundamental understanding of thermal stability, so that fuel specifications can be determined and fuel performance predicted. The thermal stability of fuels has been a topic of study for many years (1-41). Several techniques, e.g., adjustment of fuel physical and chemical properties, exclusion of oxygen, addition of chelating agents, etc. have been considered to enhance fuel stability. While empirical evidence has been obtained about the effects of various contaminants and environmental parameters on fuel performance for a given fuel, relatively little is known about the mechanisms involved. In addition, there is limited understanding of the thermal stability of jet fuels at supercritical conditions (36).

In the practical application of fuels in advanced aircraft, the most important consideration is to know under what circumstances the fuel will degrade to the extent that a deposit is formed. A lot of effort has been devoted to the development of additives to enhance fuel stability. However, the testing of these additives and the formulation of thermally stable fuels has been hindered by the lack of reliable instrumentation and test methods to evaluate these fuels.

2.2. The Innovations

The innovation offered in the Phase II proposal (42) is the development of the next generation Fuel Stability Test System (FSTS) based on multiple optical diagnostics coupled with advanced data analysis methods. Such an approach allows one to measure thermal stability as a response surface in n-dimensional space, which is required to capture the complexity and richness of the data and the unique characteristics of each fuel. This approach also has the potential to significantly reduce the measurement times for fuel stability determinations (from hours to minutes). The optical diagnostic methods used will be FT-IR spectroscopy and its complement, FT-Raman spectroscopy, which are uniquely suited for this task.

Previous work at Advanced Fuel Research, Inc. (AFR) has demonstrated the value of on-line FT-IR diagnostics for monitoring fuel thermal stability (17-19,28,29). The initial studies utilized two cells in series after the heated zone (17-19). The first cell was an FT-IR attenuated total reflectance (ATR) cell which monitored changes in the bulk fuel composition due to thermal stressing (17,18). Changes in aromatic and olefinic bands correlated with the formation of soluble gums for two fuels (JP-5, dodecane). The second cell was a 1 mm pathlength FT-IR transmission cell. This cell was used to monitor the concentration of carbonyl groups, which went through a maximum in the same temperature range as the deposit formation rate in the case of aerated JP-5. However, the cell dimensions and the spectral analysis software were not optimized to determine whether good quantitation and discrimination of individual carbonyl compounds (aldehydes, ketones) and dissolved gases could be achieved. A second study focused on direct measurement of the deposit formation process by using a sapphire ATR fiber in the heated zone (28,29). This technique was able to detect deposit formation based on changes in the CH_2/CH_3 ratio, which confirmed previous (off-line) measurements indicating the aliphatic character of the initial deposits (17,18).

The current Phase I program resulted in the development of FT-IR Fiber Optic transmission cells for measurement of oxygenated species and a methodology for measuring deposit forming tendencies by the perturbations of FT-IR transmission measurements when an in-line filter is used.

The use of these multiple optical techniques in combination with advanced data analysis methods such as artificial neural networks should allow more reliable indices of thermal and oxidative stability to be developed. An analogy can be made to the problem of fire detection. It has been found that an index developed from a combination of smoke, CO_2, and CO detectors is much more reliable than any of the individual measurements (43). The problem of measuring fuel thermal stability has typically involved single parameter measurements and the results have not always been reliable or consistent from one test to the next (44).

2.3 Summary of Phase I Accomplishments

The Phase I program has demonstrated the capability of FT-IR Fiber Optic Transmission (FOT) spectroscopy to make in-situ measurements of oxygenated species (CO_2, alcohols, carbonyls) known to be involved in fuel degradation processes and to provide reliable indications of fuel oxidative and thermal stability. The specific accomplishments of this program can be summarized as follows:

- Designed, constructed, and tested an improved Fuel Stability Test System with three high pressure in-situ fiber optic transmission cells (2 mid-infrared, 1 near-infrared)

- Designed, constructed, and tested a multiple path optical bench that could switch between the three fiber optic cells using computer controlled mirrors

- Made in-situ IR transmission measurements of peroxide decomposition products from stressed fuels including carbonyls (free and acid form), alcohols, and CO_2 (two forms). The measurements of CO_2 are believed to be the first reported measurements in a stressed jet fuel.

- Demonstrated that the IR transmission measurements are consistent with the generally accepted free radical mechanism of fuel degradation, including the inverse relationship between oxidative and thermal stability.

- Demonstrated a methodology for predicting the deposit forming tendencies by the perturbations of FT-IR transmission measurements when an in-line filter is used, which agrees well with results from the literature.

- Demonstrated that both the large gap (1 mm) and small gap (0.1 mm) IR transmission measurements were very sensitive to the presence of a steel wire probe in the quartz-lined thermal stressing reactor, which was consistent with significant changes in soluble gum formation that were also observed with the wire present.

- Began evaluation of FT-Raman measurements in option task which led to the preliminary conclusion that a surface enhanced probe would be desirable for monitoring fuel degradation.

2.4 Phase II Proposal

The Phase II proposal is to develop a prototype instrument which uses advanced optical diagnostics to evaluate the thermal and oxidative stability of hydrocarbon aviation fuels, including supercritical fuels. The Phase I program has demonstrated the capability of FT-IR Fiber Optic Transmission spectroscopy to make in-situ measurements of oxygenated species known to be involved in fuel degradation and to provide reliable indicators of fuel thermal and oxidative stability. The Phase II program will combine this technique with previously developed diagnostics for surface deposits such as FT-IR Fiber Optic/Attenuated Total Reflectance (FO/ATR) spectroscopy or Surface Enhanced Raman Spectroscopy (SERS) into an advanced Fuel Stability Test System (FSTS). The FSTS will be used to make measurements for a suite of fuels and establish a database for methodology and model development. Advanced data analysis techniques, such as artificial neural networks (ANN), will be used to combine the multiple diagnostic measurements into a meaningful index of fuel oxidative or thermal stability.

2.5. Expected Results

If carried through Phases II and III, this program will result in an instrument package, including software, for measurement of jet fuel thermal stability based on multiple optical methods. The program is designed to produce an instrument that will have direct application to process development activities for thermally stable fuels and supercritical fuels for hypersonic aircraft. However, the same instrument would have applications in a much wider market such as the production of gasoline which does not clog fuel injectors and the assessment of heat exchanger fouling in the petrochemical industry. A recent study at Argonne National Laboratory estimates that fouling costs a typical 100,000 barrel/day refinery ~ $14 million per year in increased energy and maintenance costs (45). Similarly, a British study estimated the annual cost of heat exchanger surface fouling in industry as being equivalent to about 0.3% of the U.K. Gross National Product (46). The successful development of the advanced FSTS based on optical diagnostics would provide the following benefits which have commercial value: 1) A quantitative and reliable instrument for rapid measurement of fuel to thermal and oxidative stability 2) The possibility of on board monitoring of deposit buildup in aircraft engines and fuel supply systems; 3) Improved global models of fuel degradation mechanisms; 4) a knowledge base to design stable fuels or make a priori predictions of fuel stability based on composition. A follow-on funding agreement has been obtained from On-Line Technologies, Inc. (On-Line) for the Phase III program.

3. IDENTIFICATION OF THE PROBLEM AND OPPORTUNITY

3.1. The Problem

The fuel is utilized as a primary heat sink on most aircraft. Consequently, the development of advanced high speed aircraft using hydrocarbon fuels will require fuels which have very high thermal stability, including fuels which can be stable above the critical temperature and pressure. In addition, the expected transition to fuels from new sources will require a more fundamental understanding of thermal stability, so that fuel specifications can be determined and fuel performance predicted. The thermal stability of fuels has been a topic of study for many years (1-41). Several techniques, e.g., adjustment of fuel physical and chemical properties, exclusion of oxygen, addition of chelating agents, etc. have been considered to enhance fuel stability. While empirical evidence has been obtained about the effects of various contaminants and environmental parameters on fuel performance for a given fuel, relatively little is known about the mechanisms involved. In addition, there is limited understanding of the thermal stability of jet fuels at supercritical conditions (36).

In the practical application of fuels in advanced aircraft, the most important consideration is to know under what circumstances the fuel will degrade to the extent that a deposit is formed. A lot of effort has been devoted to the development of additives to enhance fuel stability. However, the testing of these additives and the formulation of thermally stable fuels has been hindered by the lack of reliable instrumentation and test methods to evaluate these fuels.

3.2. The Innovations and Opportunity for Solution

The innovation offered in the Phase II proposal (42) is the development of the next generation Fuel Stability Test System (FSTS) based on multiple optical diagnostics coupled with advanced data analysis methods. Such an approach allows one to measure thermal stability as a response surface in n-dimensional space, which is required to capture the complexity and richness of the data and the unique characteristics of each fuel. This approach also has the potential to significantly reduce the measurement times for fuel stability determinations (from hours to minutes). The optical diagnostic methods used will be FT-IR spectroscopy and its complement, FT-Raman spectroscopy, which are uniquely suited for this task.

Previous work at Advanced Fuel Research, Inc. (AFR) has demonstrated the value of on-line FT-IR diagnostics for monitoring fuel thermal stability (17-19,28,29). The initial studies utilized two cells in series after the heated zone (17-19). The first cell was an FT-IR attenuated total reflectance (ATR) cell which monitored changes in the bulk fuel composition due to thermal stressing (17,18). Changes in aromatic and olefinic bands correlated with the formation of soluble gums for two fuels (JP-5, dodecane). The second cell was a 1 mm pathlength FT-IR transmission cell. This cell was used to monitor the concentration of carbonyl groups, which went through a maximum in the same temperature range as the deposit formation rate in the case of aerated JP-5. However, the cell dimensions and the spectral analysis software were not optimized to determine whether good quantitation and discrimination of individual carbonyl compounds (aldehydes, ketones) and dissolved gases could be achieved. A second study focused on direct measurement of the deposit formation process by using a sapphire ATR fiber in the heated zone (28,29). This technique was able to detect deposit formation based on changes in the CH_2/CH_3 ratio, which confirmed previous (off-line) measurements indicating the aliphatic character of the initial deposits (17,18).

The current Phase I program resulted in the development of FT-IR Fiber Optic transmission cells for measurement of oxygenated species and a methodology for measuring deposit forming tendencies by the perturbations of FT-IR transmission measurements when an in-line filter is used.

The use of these multiple optical techniques in combination with advanced data analysis methods such as artificial neural networks should allow more reliable indices of thermal and oxidative stability to be developed. An analogy can be made to the problem of fire detection. It has been found that an index developed from a combination of smoke, CO_2, and CO detectors is much more reliable than any of the individual measurements (43). The problem of measuring fuel thermal stability has typically involved single parameter measurements and the results have not always been reliable or consistent from one test to the next (44).

4. PHASE I OBJECTIVES

The overall objective of the Phase I proposal was to develop a methodology for on-line optical measurements of peroxide decomposition products and demonstrate how this information could be used to elucidate the chemical mechanisms of fuel degradation. The work was done in four tasks with the following specific objectives.

Task 1 - Optical Cell Design, Construction and Testing - An optical cell will be designed which will allow for simultaneous measurements of peroxide decomposition products by FT-IR transmission and FT-NIR spectroscopy.

Task 2 - Thermal Stressing Experiments - Experiments will be performed over a range of fuel stressing conditions (including supercritical) to examine the effects of fuel type, temperature, and oxygen concentration. On-line measurements of fuel composition will be made with the diagnostics developed in Task 1. Off-line measurements of deposit formation rates and gum concentrations (soluble and insoluble) will also be made.

Task 3 - Data Interpretation and Modeling - Data developed in Task 2 will be analyzed along with existing data and models in order to develop a quantitative model that can describe fuel degradation at temperatures up to 400 °C. The model would be formulated under the Phase I program but would not be extensively tested until Phase II.

Task 4 - Investigation of On-line Raman Monitors (Option) - Assessment of FT-Raman spectroscopy as an on-line monitor for the bulk composition of stressed fuels.

5. PHASE I RESULTS

5.1 Task 1 - Optical Cell Design, Construction and Testing

Objective

An optical cell will be designed which will allow for simultaneous measurements of peroxide decomposition products by FT-IR transmission and FT-NIR spectroscopy.

Methodology

FT-IR Transmission Spectroscopy - A previous program demonstrated the application of FT-IR diagnostics for the on-line monitoring of fuel composition (17,18). Both a SpectraTech Attenuated Total Reflectance (ATR) circle cell and a 1 mm path transmission cell were used in series. However, the pressure was reduced before passage into the transmission cell. The question arose as to whether some important fuel characteristics at high pressure, such as dissolved oxygenated gases or light oxygenated compounds, are missing at one atmosphere. Therefore, a high pressure cell was designed under the current program for making the FT-IR and FT-NIR measurements.

A second requirement is that the transmission cell have a variable pathlength. In the previous work, a fixed 1 mm pathlength was used since this was available commercially. This was adequate for making semi-quantitative measurements of total carbonyl content, but information on alcohols or ethers was not available from these spectra and the peaks could not be resolved into aldehyde and ketone contributions. The pathlength must be optimized to maximize sensitivity and minimize interference and this will require a variable pathlength cell. A third requirement is improved data analysis techniques for curve resolving. The ability to rapidly design and test curve resolving alogorithms has been greatly improved by the availability of PC-based spectral manipulation packages such as Spectra-Calc (Galactic Industries). These were used for curve resolving and quantitation of the FT-IR transmission spectra.

Near Infrared (NIR) Spectroscopy - NIR spectroscopy has been used in the agricultural industry for quite some time as a tool for quantitating moisture content in grains (47). Recent advances in instrumentation, computers, and data analysis methods have resulted in a large upsurge in the use of NIR analysis for applications such as the determination of moisture, starch, and protein contents in foods, the determination of octane number, vapor pressure, and a variety of physical parameters in gasolines (47,48), and both quantitative analysis and quality control of pharmaceutical raw materials and finished products (49,50). Additionally, field and process monitoring applications have increased greatly due to the capability to rapidly determine process variables. The success of NIR analyses in the petroleum industry suggests that this technique may be useful in the monitoring of jet fuel degradation.

Absorption bands that are observed in the NIR spectra of organics are overtones and combinations of the fundamental bands typically present in the mid-IR spectra (51,52). *Fundamental bands* are transitions from the ground vibrational state to the first excited state (v=1, where v is the vibrational quantum number). *Overtone bands* are transitions from the ground state to the second and higher vibrational states (Δv=2,3,...). *Combination bands* are observed when two vibrational modes are excited by a single photon. The frequency of these bands corresponds to the sum of the energies of the two vibrational transitions. Combinations become allowed as a result of the coupling of the two molecular vibrations within the molecule. While overtones and combinations are typically quite weak compared to fundamentals, this is not necessarily a disadvantage. Lower absorptivities allow for longer pathlengths, thus reducing the stringent sampling requirements of mid-IR spectroscopy. There are certain advantages to working in the

NIR spectral region (1.0-2.5 μm): glass optics and sample cells do not interfere; NIR fiber optics are off-the-shelf items; signal to noise ratios are better due to the higher sensitivity of typical NIR detectors. However, NIR spectra of organics typically exhibit fairly broad overlapped bands, and are often difficult to interpret. Until recently, this complexity has prevented the extensive use of the wealth of information present in the NIR. The development of chemometrics has provided data analysis techniques that are capable of objectively extracting information for use in quantitative calibrations or discriminant analysis. Common methods for developing quantitative calibrations are partial least squares (PLS), (53) principal components regression (PCR), (54) classical least squares (CLS), (55) and inverse least squares (ILS) (56).

Work Performed

Construction of Transmission Cells and Multiple Path Optical Bench - The transmission cells were designed to be installed after the heated zone in a Fuel Stability Test System (FSTS) that was developed at AFR in two previous Air Force Phase I SBIR programs (17,28). The system was assembled from relatively low cost, modular, high pressure liquid chromatography (HPLC) components. Photographs of the complete FSTS are shown in Fig. 5.1-1, while Fig. 5.1-2 shows closeup photographs of the two IR transmission cells. A similar design was used for the NIR cell. Figure 5.1-3 shows a block diagram of the system that was constructed. Fuel is delivered via standard plumbing to a heated assembly which can accommodate a sapphire fiber optic ATR sensor. That sensor was not installed during the current Phase I program since it was demonstrated in a previous Phase I program (28) and the optical bench for the spectrometer could only accommodate three detectors. The fuel is thermally stressed in the furnace and then flows through a filter (optional) and three high pressure transmission cells installed in series. Note that the back pressure regulator is mounted downstream of the transmission cells so that all measurements are made prior to pressure reduction.

Each transmission cell consists of a 1/16" cross with polished fiber optics installed in opposed ports using either graphite or Vespel/graphite ferrules to create a high pressure seal, as shown in Fig. 5.1-4a. The use of fiber optics was motivated by the desire to have high pressure cells with adjustable pathlengths. In the case of the IR cells, chalcogenide fibers (Amorphous Materials, Inc.) were used with the cladding. Since these fibers are too soft to be directly sealed using a compression fitting, they were bonded into 1/16 inch stainless steel tubes using epoxy, as shown in Fig. 5.1-4b. Stainless steel ferrules were then used to seal these tubes to the fittings. The next step was to polish the ends of the fibers and set the gap between the two ends inside the cell. The optical pathlength of the transmission cell is controlled by adjusting the gap between the two fibers. Several combinations of cell pathlength, fiber material, and detector type can be selected depending upon the type of measurement that is desired. A list of possible relevant applications and configurations is included in Table 5.1-1. Under the current program, two FT-IR transmission cells, were constructed using chalcogenide fibers and 1.0 mm and 0.1 mm nominal pathlengths, respectively. A DTGS infrared detector was mated to the assembly with the output fiber positioned directly adjacent to the detector element, as shown in Fig. 5.1-4a. The same design was used for the small gap and large gap IR cells. In the case of the NIR cell, silica fibers and an InSb detector were used. Since the InSb detector is liquid nitrogen cooled, it cannot be mounted directly on the cell and the connection is made using a light pipe.

A schematic of the optical system is shown in Figure 5.1-5. The three cells were mounted on the baseplate of a Bomem FT-IR spectrometer, and a series of flipper mirrors was used to direct the infrared beam to the selected cell. This allows for the three cells to be sequentially scanned using the same spectrometer. The FT-IR spectrometer computer is used to control the rotatable paraboloidal flipper mirrors. The work in Task 1 was done with a Bomem M155 spectrometer at a resolution of 4 cm^{-1}. At the beginning of Task 2, a switch was made to a Bomem M100, which was

a

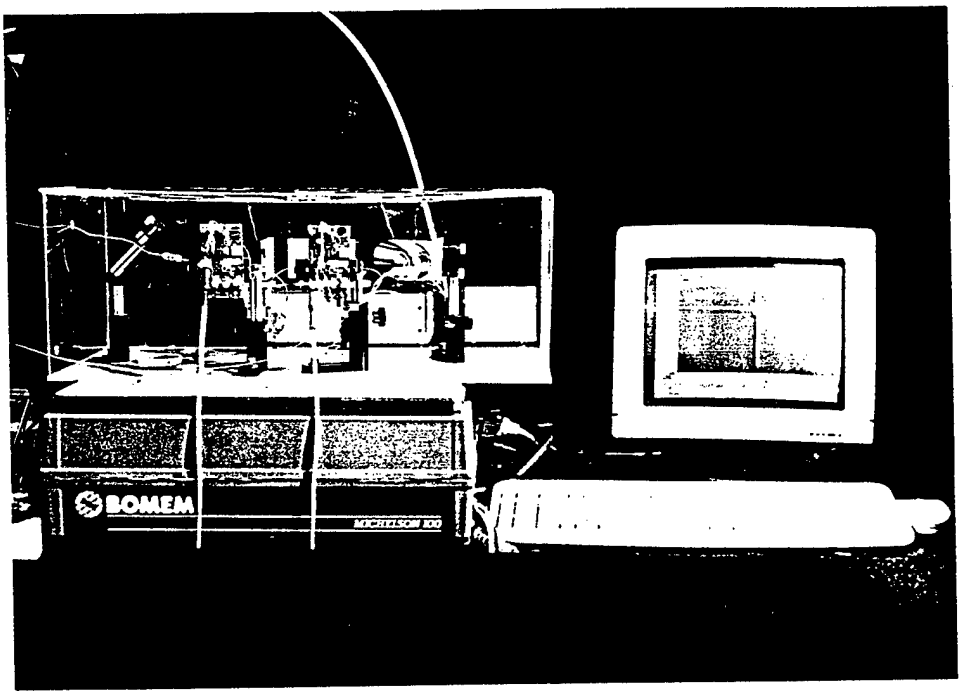

b

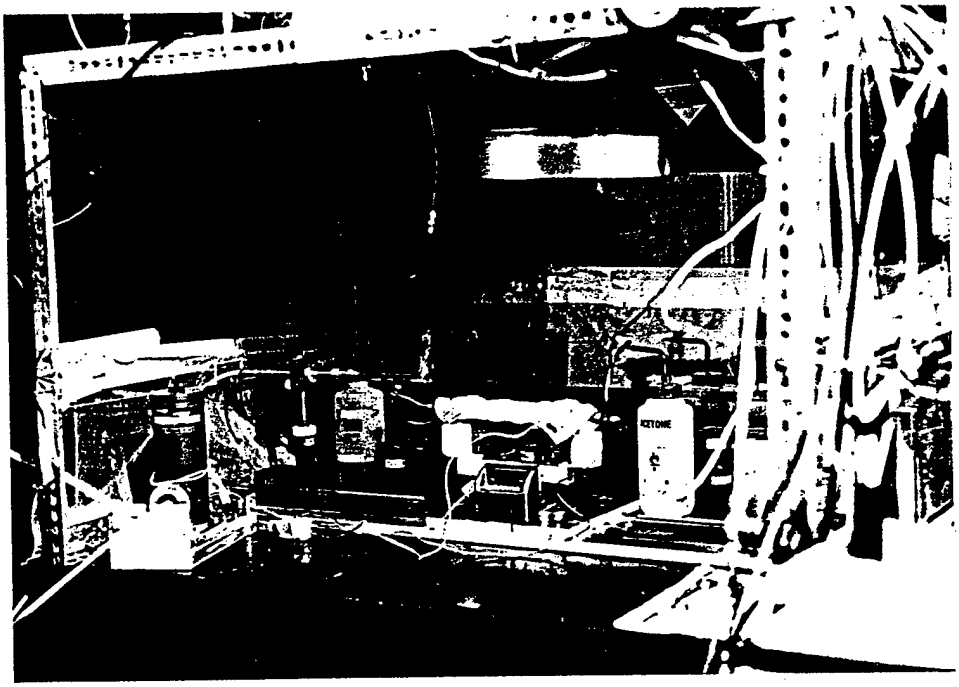

Figure 5.1-1. Photographs of Fuel Stability Test System. a) View of Computer, Spectrometer, and Cell Compartment; b) View of the Heated Thermal Stressing Reactor Inside a Ventilated Hood. The Valve and Pump System are Located above the Hood, while the Spectrometer is to the Right

a

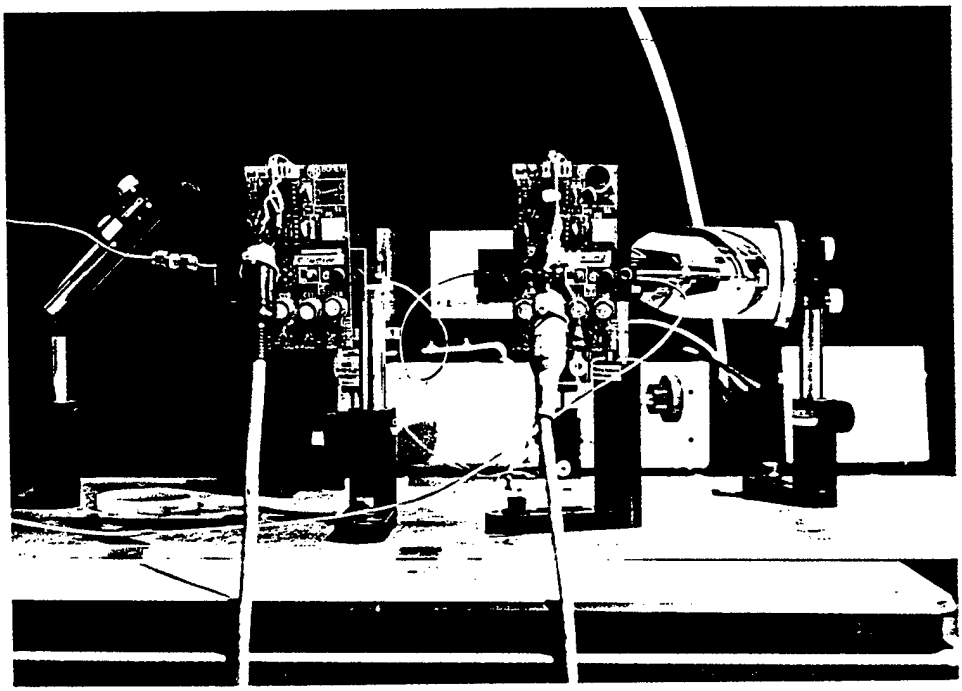

b

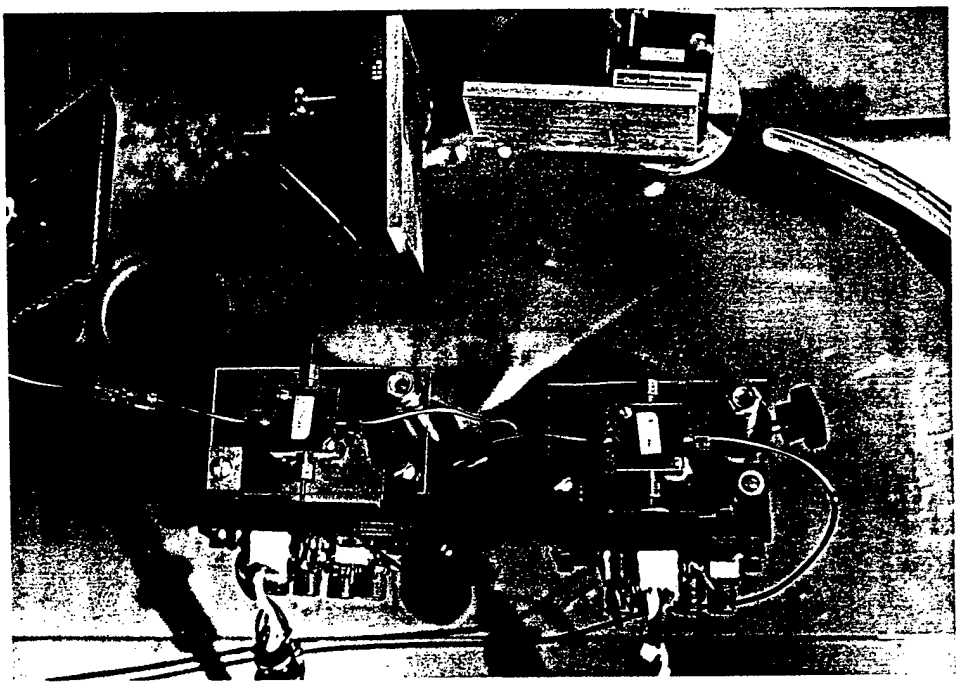

Figure 5.1-2. Close-up Photographs of the Optical Cell Compartment for the Fuel Stability Test System. a) Side View of the Optical Cell Compartment Showing the Two DTGS Detectors; b) Top View of the Optical Cell Compartment Showing the Small Gap (0.1 mm) and Large Gap (1.0 mm) Cells, the Computer-Controlled Mirror System and the IR Port. The Optics in the Photograph are in Position to Focus the IR Light on the Small Gap (left) Cell.

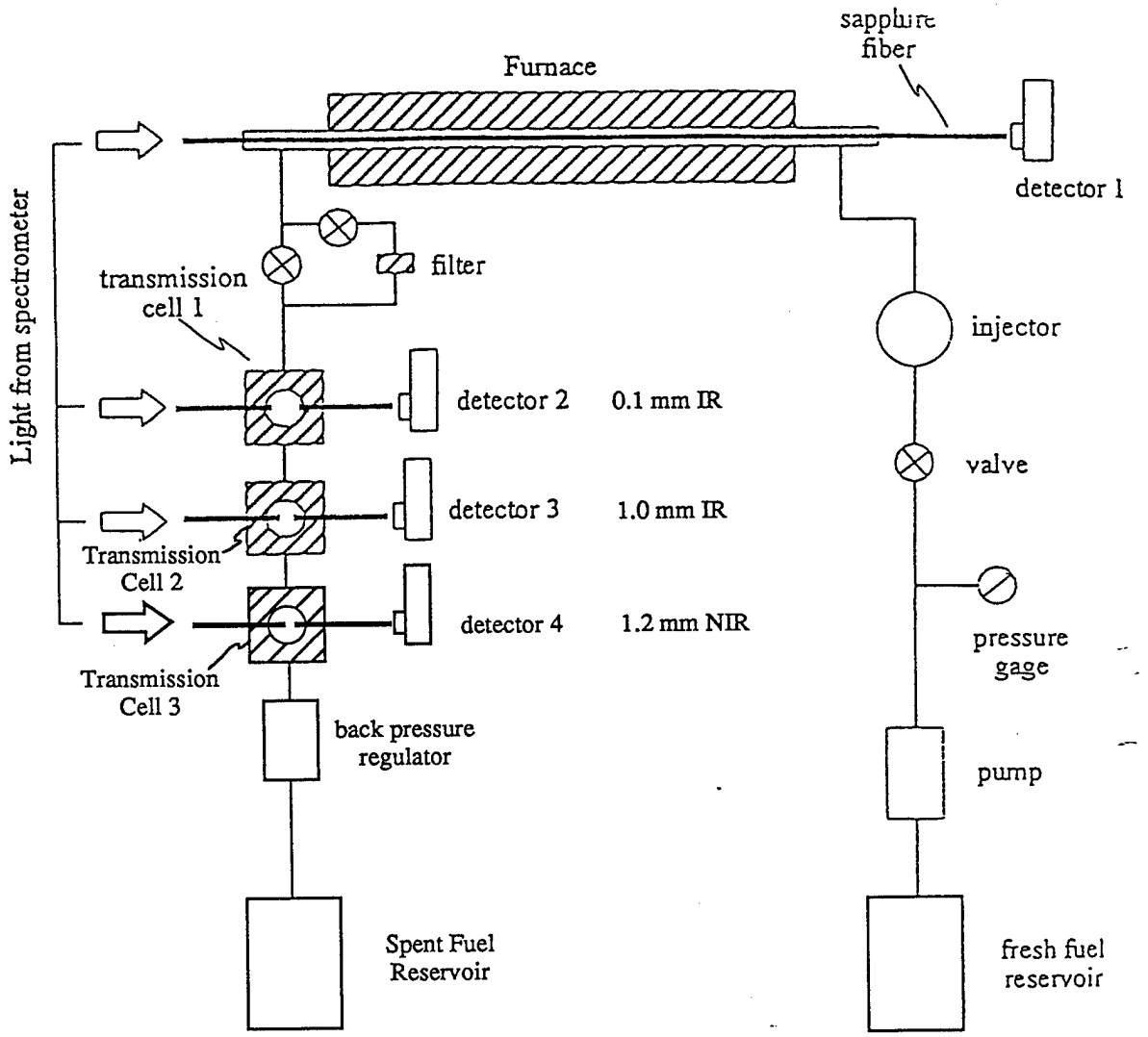

Figure 5.1-3. Block Diagram of the System Assembled during the Phase I Program. Standard Plumbing is used to Deliver the Fuel to the Thermal Stressing Furnace which Can Also Incorporate a Sapphire Fiber Optic ATR Sensing Element Which was not Installed during the Current Program. The Fuel then Passes through a Filter (optional) and Three High Pressure Fiber Optic Transmission Cells. The Transmission Cells can be Configured for Several Different Types of Measurements.

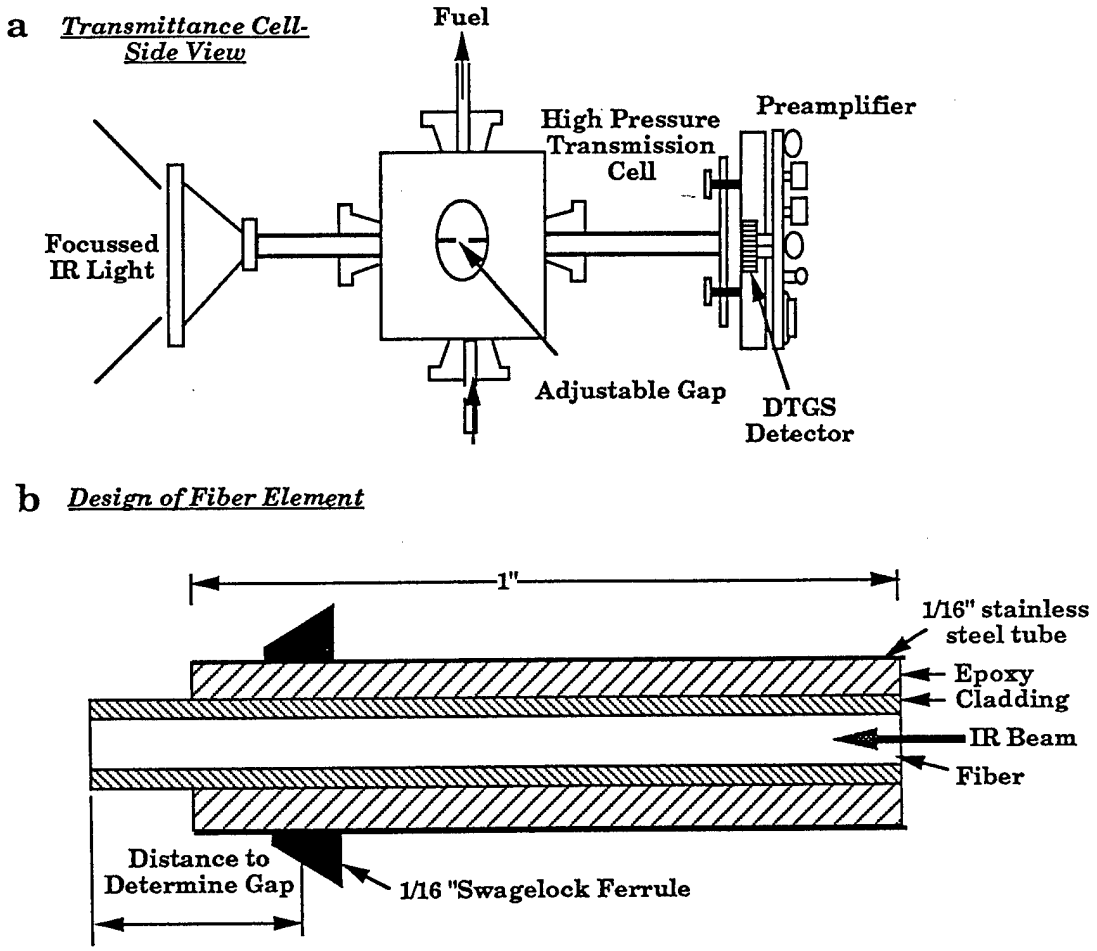

Figure 5.1-4. The High Pressure Fiber Optic Transmission Cell Consists of a 1/16" Cross with Polished Fibers Installed in Opposed Ports. The Optical Pathlength of the Transmission Cell is Controlled by Adjusting the Gap Between the Two Fibers. Several Combinations of Cell Pathlength, Fiber Material, and Detector Type can be Selected Depending Upon the Type of Measurements that is Desired.

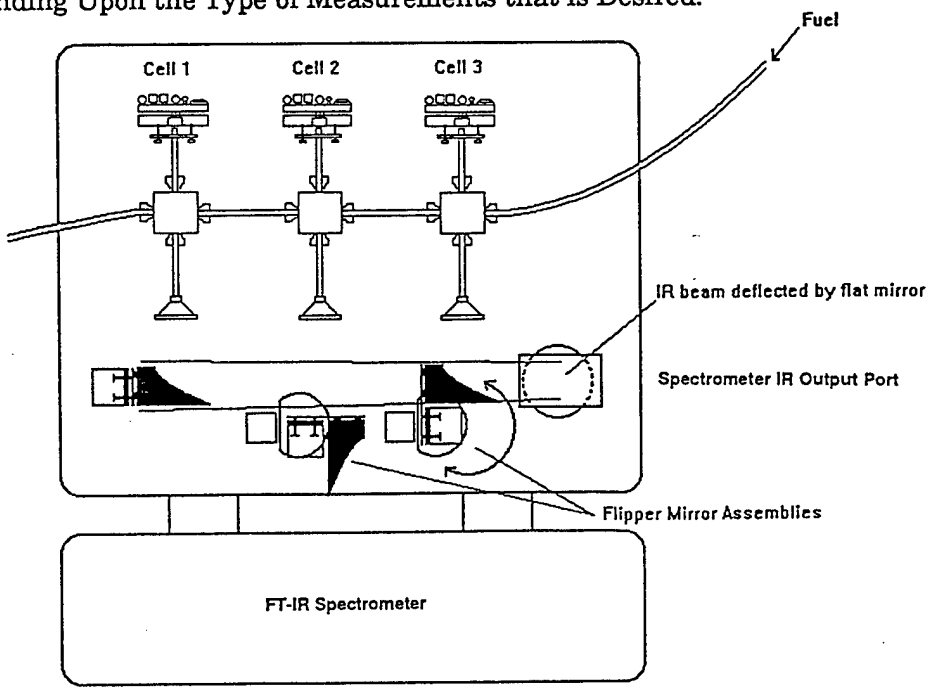

Figure 5.1-5. Schematic Showing the Operation of the Computer Controlled Mirrors. The Beam from the Spectrometer can be Focussed onto One of Three Cells by Appropriately Positioning the Rotatable Paraboloidal Mirrors.

also operated at 4 cm^{-1} resolution, since the variable resolution M155 was required for a different project.

Table 5.1-1. Potential measurement types and the corresponding configurations for the high pressure fiber optic transmission cells

Measurement Type	Spectral Range	Pathlength	Fiber	Detector
hydrocarbons	3,500-1,000 cm^{-1}	0.05 mm	chalcogenide	DTGS / MCT
hydrocarbons	8,000-4,500 cm^{-1}	1.0 mm	silica	InSb / InGaAs
hydrocarbons	12,000-8,000 cm^{-1}	2.0 mm	silica	Si
carbonyls	1,800-1,600 cm^{-1}	1.0 mm	chalcogenide	DTGS / MCT
alcohols	4,000-3,000 cm^{-1}	0.1 mm	chalcogenide	InSb / MCT
alcohols	8,000-4,000 cm^{-1}	1.0 mm	silica	InSb / InGaAs
alcohols	12,000-8,000 cm^{-1}	2.0 mm	silica	Si
ethers	1,500-1,000 cm^{-1}	0.1 mm	chalcogenide	DTGS / MCT

Testing of Transmission Cells - Mid-infrared spectra collected using the cells with chalcogenide fibers and two different pathlengths (0.1 mm and 1.0 mm) are shown in Figure 5.1-6 for the Sun Jet A-1 (#2747) jet fuel. It can be seen that the small gap cell provides a spectrum of the whole fuel (Fig. 5.1-6a) while the large gap cell is saturated in most regions (Fig. 5.1-6b). The plan for Phase I was to use three transmission cells in series to measure spectra of the stressed fuel. Two of the cells were configured for the mid-infrared (chalcogenide fiber, DTGS detector), one with a short pathlength (0.05-0.10 mm) for monitoring high concentration constituents, and one with a long pathlength (~1.0 mm) for monitoring low concentration degradation products. The third cell was configured for the near infrared (silica fiber, InSb detector) with a 1.2 mm pathlength for monitoring the bulk composition of the stressed fuel. All three cells held pressure to 3000 psi.

Methyl t-butyl ether (MtBE) and acetone were used in unstressed Sun super K-1 jet fuel to determine the optical sensitivity of the system for the presence of ketone and ether constituents. These model compounds are representative of products from the fuel peroxide degradation. Spectra collected using the mid-infrared cells using two different pathlengths (0.1 mm and 1 mm) for MtBE doped jet fuel are shown in Figs. 5.1-7 and 5.1-8. These spectra are ratioed to the undoped fuel. Figure 5.1-7a shows a bulk absorbance spectrum for the lower mid-infrared region in the 0.1 mm chalcogenide transmission cell for two concentrations of MtBE in jet fuel. Figure 5.1-7b shows an expanded spectral region for the same cell at high wavenumbers which demonstrates the ability of the 0.1 mm cell to follow bulk changes in the aliphatic components of the fuel. Figure 5.1-8 is a partial absorbance spectrum of 0.1% MtBE in jet fuel in the 1 mm pathlength cell relative to the undoped fuel. Note the negative peaks just above 1600 and 1500 cm^{-1} are due to replacement of aromatic fuel components with dopant.

Spectra collected for two concentrations (0.1 and 1.0 % volumetric) of acetone doped jet fuel in the three cells are shown in Fig. 5.1-9, also plotted relative to the undoped fuel. Figure 5.1-9a shows the mid-infrared region which includes absorbance bands of the carbonyl and aromatic peaks. The absorbance at 1734 cm^{-1} is the carbonyl peak of the acetone and the two negative peaks at 1512 and 1605 cm^{-1} are the aromatic peaks due to replacement of the fuel.

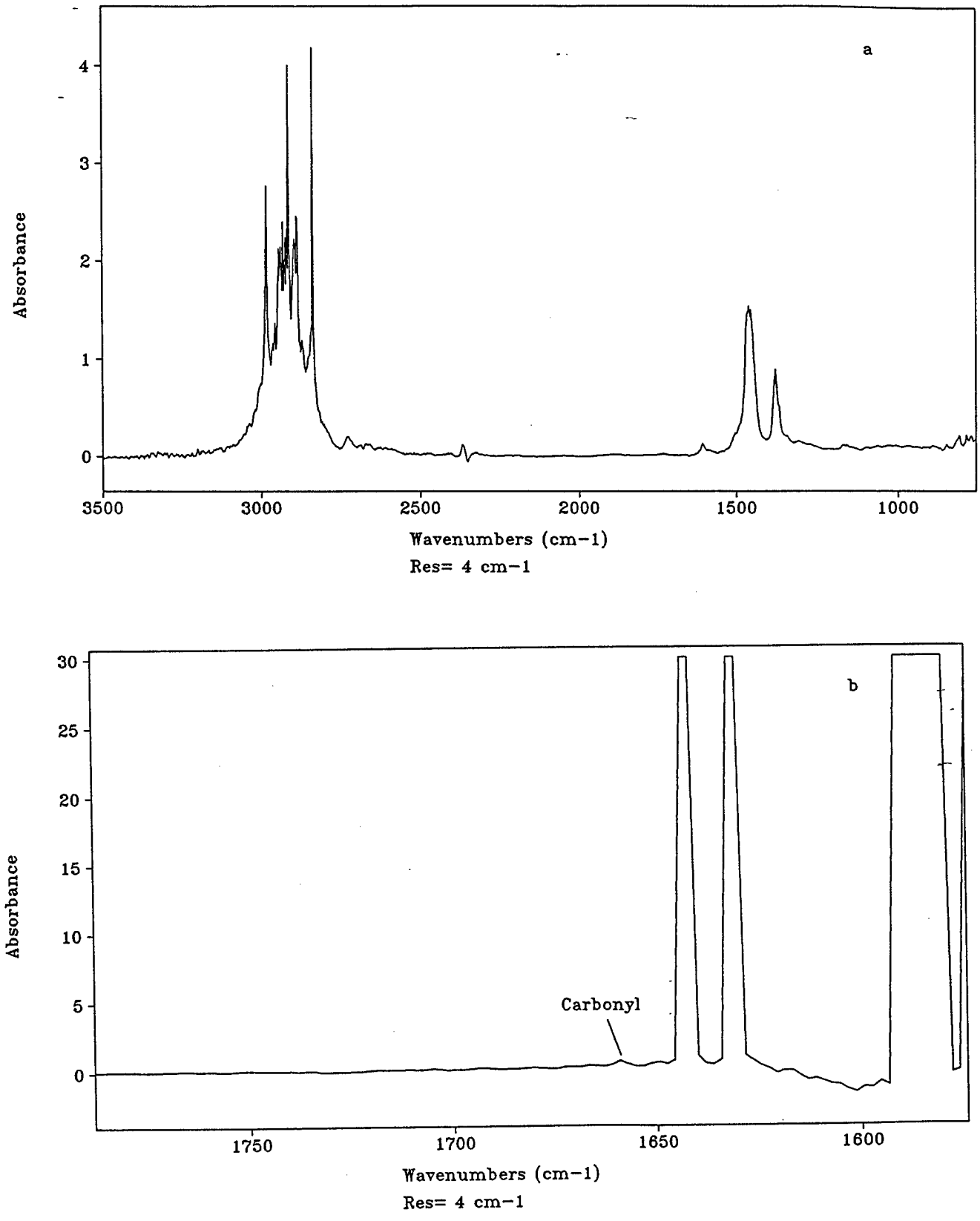

Figure 5.1-6. Mid-Infrared Spectra of Sun Jet Fuel Obtained using the Fiber Optic Transmission Cell with a) 0.1 mm Pathlength and b) 1.0 mm Pathlength using Chalcogenide Fibers and a DTGS Detector.

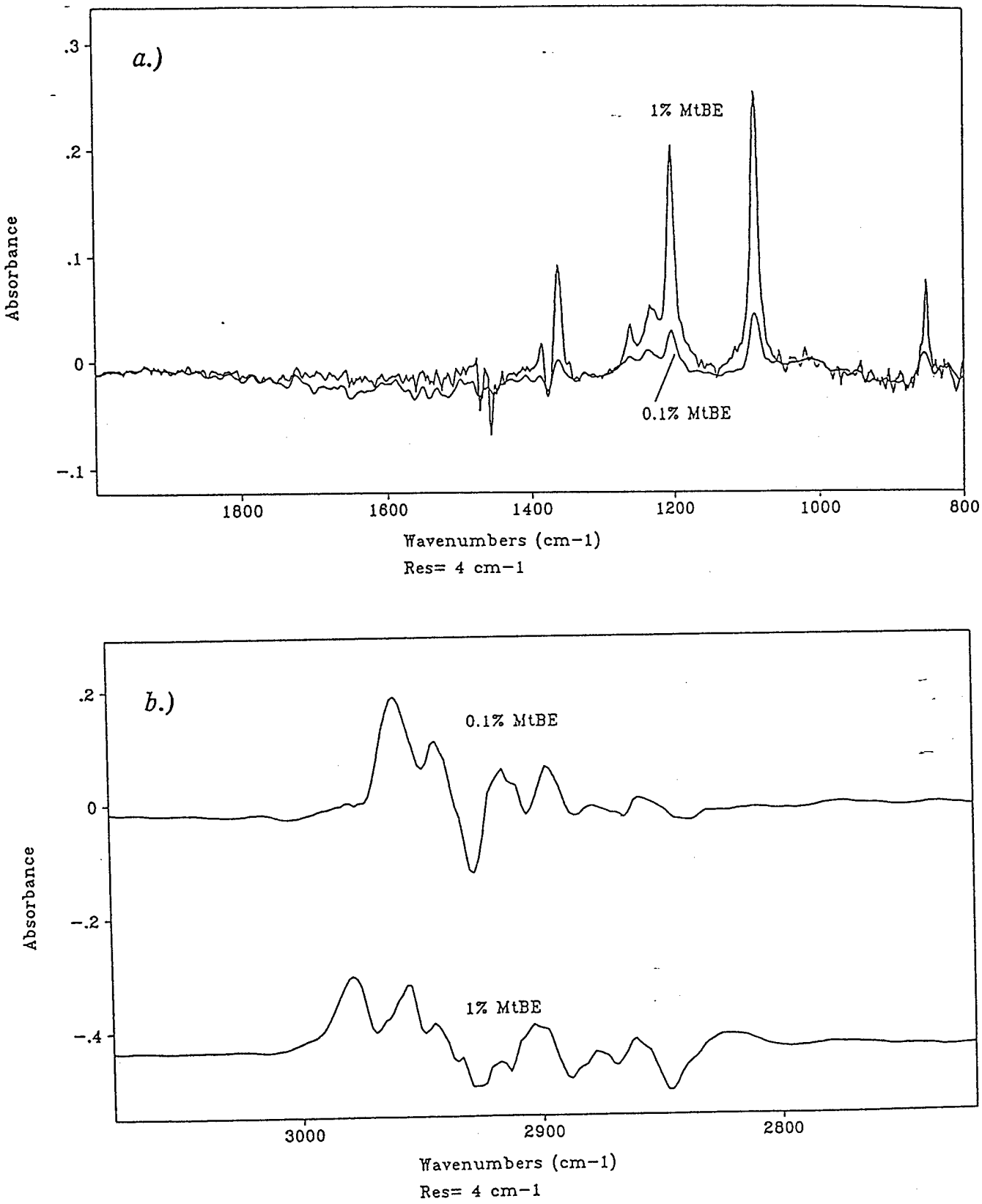

Figure 5.1-7. Mid-Infrared Absorbance Spectra for Two Concentrations of MtBE Doped Jet Fuel Obtained Using the Fiber Optic Transmission Cell with 0.1 mm Pathlength Using Chalcogenide Fibers and a DTGS Detector. a) Low Wavenumber Range Showing Bulk Properties of Doped Fuel; b) High Wavenumber Range Showing Changes in Aliphatic Components with Dopant.

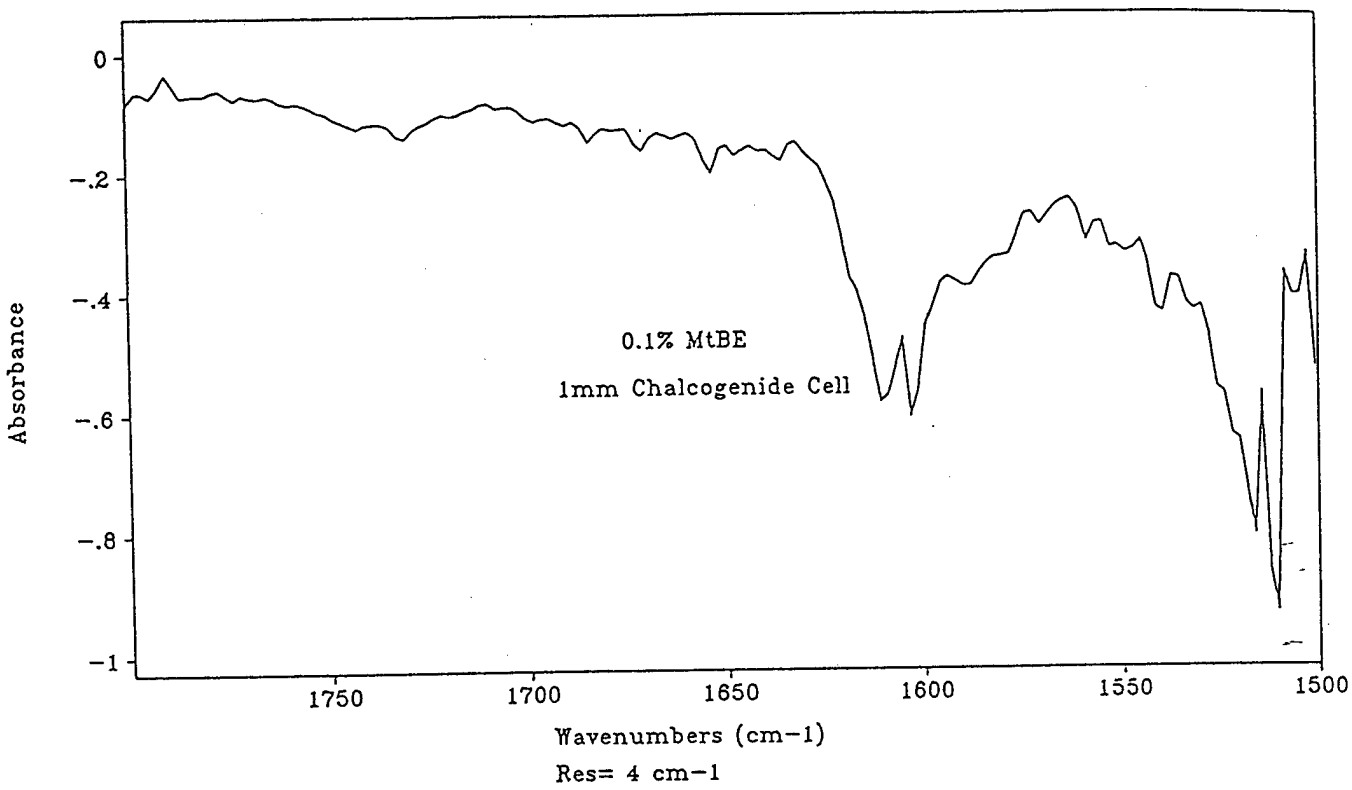

Figure 5.1-8. Mid-Infrared Absorbance Spectra for MtBE Doped Jet Fuel Obtained using the Fiber Optic Transmission Cell with 1 mm Pathlength using Chalcogenide Fibers and a DTGS Detector. The Negative Peaks are Due to Replacement of Jet Fuel with the Dopant.

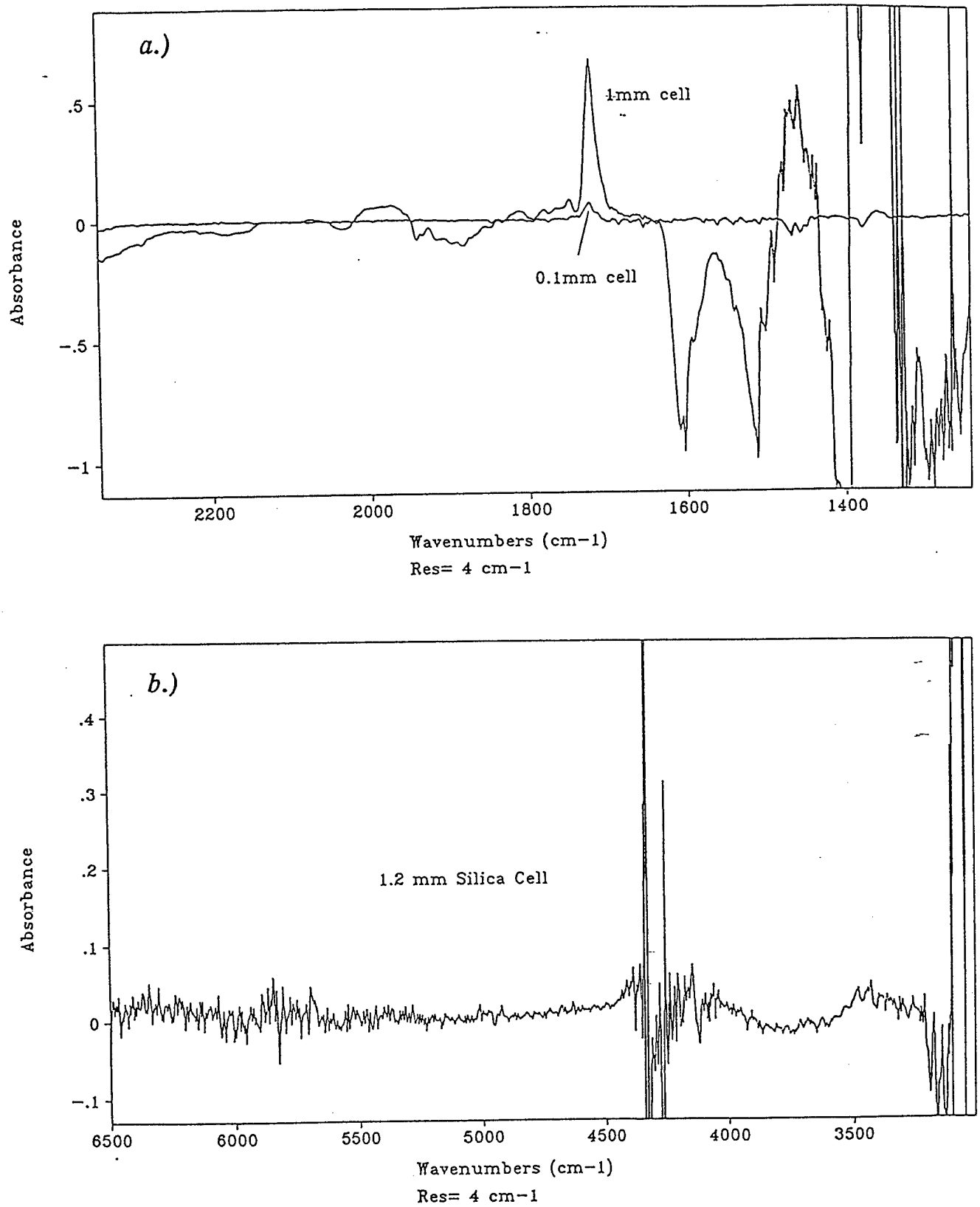

Figure 5.1-9. Overlay of Absorbance Spectra for Acetone Doped Jet Fuel Using the Fiber Optic Transmission Cell with a) Chalcogenide Fibers (at 0.1 and 1 mm pathlengths) and a DTGS Detector; b) Silica Fibers and an InSb Detector (1.2 mm pathlength).

A near-infrared (NIR) absorbance spectrum for 0.1% acetone in jet fuel in the 1.2 mm silica transmission cell is shown in Figure 5.1-9b. The silica fiber cuts off below 3200 cm^{-1}. Acetone absorbance bands are seen in the 3500 to 3200 cm^{-1} range and the 4000-4500 cm^{-1} range shows changes in the aromatic bands, including replacement of aromatics by acetone (sharp negative peaks). At the conclusion of Task 1, it was determined that the NIR transmission measurements should not be continued. The reason was due to the low sensitivity observed with our current spectrometers which are optimized for mid-IR measurements, including the use of a globar source which does not provide much energy in the NIR region. This problem could be largely solved by the use of a tungsten-halogen source, but the Bomem M100 and M155 spectrometers used could only accommodate a single source. Under the proposed Phase II program, a custom built On-line Technologies, Inc. spectrometer would be used which would not have this limitation. However, the NIR measurements would probably still require a longer pathlength and this could mean a cell with a relatively large dead volume. It was decided that the use of the NIR optics would be more appropriate once the fundamental information from the mid-IR measurements has been acquired. The use of NIR optics would be advantageous for the development of a low cost on board fuel stability monitor and will be evaluated under Phase II (Task 7) (42).

Summary of Work Done Under Task 1 - Fiber Optic cells for on-line FT-IR and FT-NIR transmission measurements were designed, constructed and tested. The ability to vary the pathlength for each measurement was incorporated into the cell. The cells were tested at pressures up to 3000 psig. Experiments were done with doped fuels to determine the measurement capabilities and sensitivities for various compounds. The small gap (0.1 mm) and large gap (1.0 mm) FT-IR cells were found to be much more sensitive to changes in the fuel than the FT-NIR cell.

5.2 Task 2 - Thermal Stressing Experiments

Objective

Experiments will be performed over a range of fuel stressing conditions (including supercritical) to examine the effects of fuel type, temperature, and oxygen concentration. On-line measurements of fuel composition will be made with the diagnostics developed in Task 1. Off-line measurements of deposit formation rates and gum concentrations (soluble and insoluble) will also be made.

Methodology

The methodology for this task was described in Section 5.1. It was similar to that employed in previous tests at AFR of on-line diagnostics (17,18,28,29). The Fuel Stability Test System (FSTS) developed at AFR and modified in Task I was used for these experiments (see Fig. 5.1-3).

Work Performed

Experimental Conditions and Procedures for On-line Spectroscopic Measurements - Experiments were done with two fuels, Shell Jet A (#2827) and the Sun Jet A-1 (#2747), which have JFTOT breakpoint temperatures of 266 and 332 °C, respectively and were used in the previous Phase I program (28,29). The experiments were done primarily at four different temperature levels (150,250,350,450 °C) and with the fuels in an aerated or deaerated state created by pulling vacuum and then purging with air or nitrogen for 30 min. The system operates at pressures from 500-700 psig, which allows the investigation of supercritical conditions, and temperatures as high as 500 °C. Higher temperatures would be possible if back pressure regulators which exceed 700 psig were available. Samples of soluble gums, insoluble gums

(filtered sediment) and deposits were collected, as described below. FT-IR spectroscopic measurements were made of the stressed fuels using the small gap (0.1 mm) and large gap 1.0 mm) transmission cells developed in Task 1. These measurements were made with and without an in-line 2 micron filter in parallel or sequential experiments done under the same conditions. Experiments were also done in the presence or absence of a wire probe used to collect deposits in the heated zone.

The thermal stressing experiments involved pumping the fuel through the reactor tube (9" x 0.25" ODx 0.12" ID) at a flow rate of 0.7 mL/min while maintaining a back pressure of 600 psig. The average residence time of the fuel in the heated zone was ~2 min. The temperature of the reactor tube was ramped from ambient to either 350 °C or 450 °C during the course of the experiment, and the stressed fuel was either filtered or not filtered before passing to the three optical cells placed in series. Infrared spectra of the filtered or unfiltered stressed fuel were acquired sequentially in each of the three cells. The single beam spectra acquired during the experiment were ratioed to a single beam spectrum of the unstressed fuel obtained before the experiment was initiated. As discussed under Task 1, the FT-NIR transmission measurements were abandoned early in the Phase I program due to a lack of sensitivity for the current spectrometer system.

Off-line Measurements of Gums and Deposits - The soluble gums were determined by vacuum distillation of a 100 ml sample of stressed fuel down to a few ml. This residue was transferred into a tared aluminum dish, dried at 180 °C and weighed. The insoluble gums were collected on a room temperature 2 micron in-line stainless steel filter after allowing 100 ml of stressed fuel to pass through. The filter element was removed from the housing, lightly rinsed with acetone and dried at 110 °C. The weight of the filter element was measured before and after to obtain the deposit weight. However, it is recognized that material which is loosely bound in the filter and/or very soluble in acetone is probably lost.

For selected experiments, a length of 24 inch steel wire was weighed, folded, placed inside the quartz insert in the heated zone, and left there until exposed to 100 ml of stressed fuel. Next, the wire was removed, ultrasonicated for 15 minutes in acetone, dried at 110 °C and weighed. In most cases, a weight loss of the steel wire was observed, probably as a result of reactions with oxygen functionalities in the fuel, oxygen and/or CO_2. The acetone was dried in an aluminum dish and the residue weighed to give the wire deposit. However, no significant wire deposit could be measured, except for the Sun fuel at 150 °C. One reason may be that the presence of the wire had a profound effect on the fuel degradation chemistry, as measured by the changes in the gum formation and the IR spectral data (see below).

Measurements of Oxygenated Species Using Large Gap Cell - Figure 5.2-1 shows the absorbance spectra (relative to the unstressed fuel) obtained for the aerated Sun fuel (filter on) using the large gap mid-IR cell (1.0 mm chalcogenide). Features are observed at 1720 cm^{-1} indicating the formation of ketones, and at 2350 cm^{-1} indicating the formation of carbon dioxide. The spectra were similar for the aerated fuel with the filter off, thus indicating that these products are soluble. For the deaerated fuel, carbon dioxide formation was also observed, but began to appear at lower temperature (see Fig. 5.2-2a). Additionally, the carbon dioxide band was observed to be split into two peaks (see Fig. 5.2-2a), one of which disappeared when the filter was on for the deaerated fuel (see Fig. 5.2-2b). These results indicate that, for the deaerated fuel, most of the carbon dioxide formed is adsorbed on the insoluble materials formed during stressing. It is believed that these are the first in-situ FT-IR measurements of CO_2 in a stressed jet fuel. It is possible to make these measurements because the FT-IR cells were designed to operate at high pressure and high sensitivity. The noticeable change in the CO_2 band between the filter on and off cases for the deaerated Sun fuel also supports the idea of using filter on/off measurements as an indicator of deposit formation tendencies (see below).

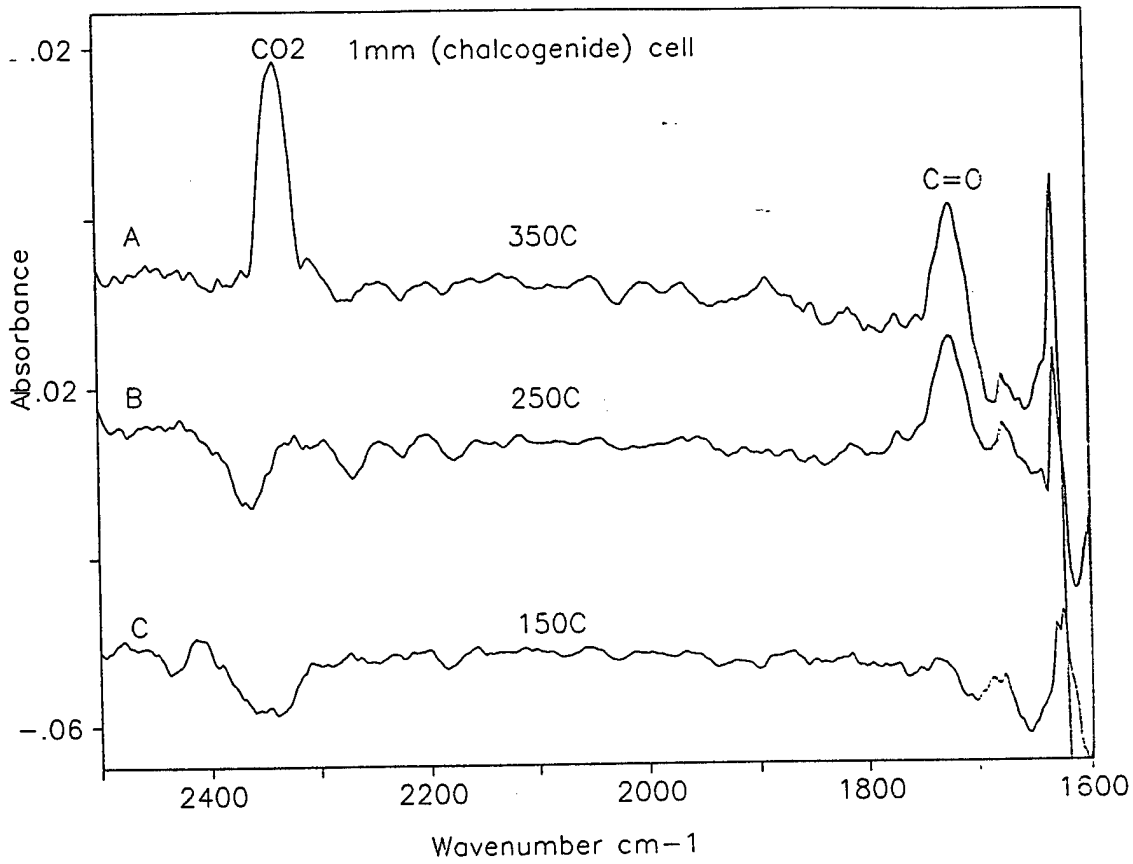

Figure 5.2-1. Absorbance Spectra Obtained During Thermal Stressing of an Aerated Sun Jet Fuel Showing the Formation of Carbon Dioxide and Ketones. In Each Case the Filter was On.

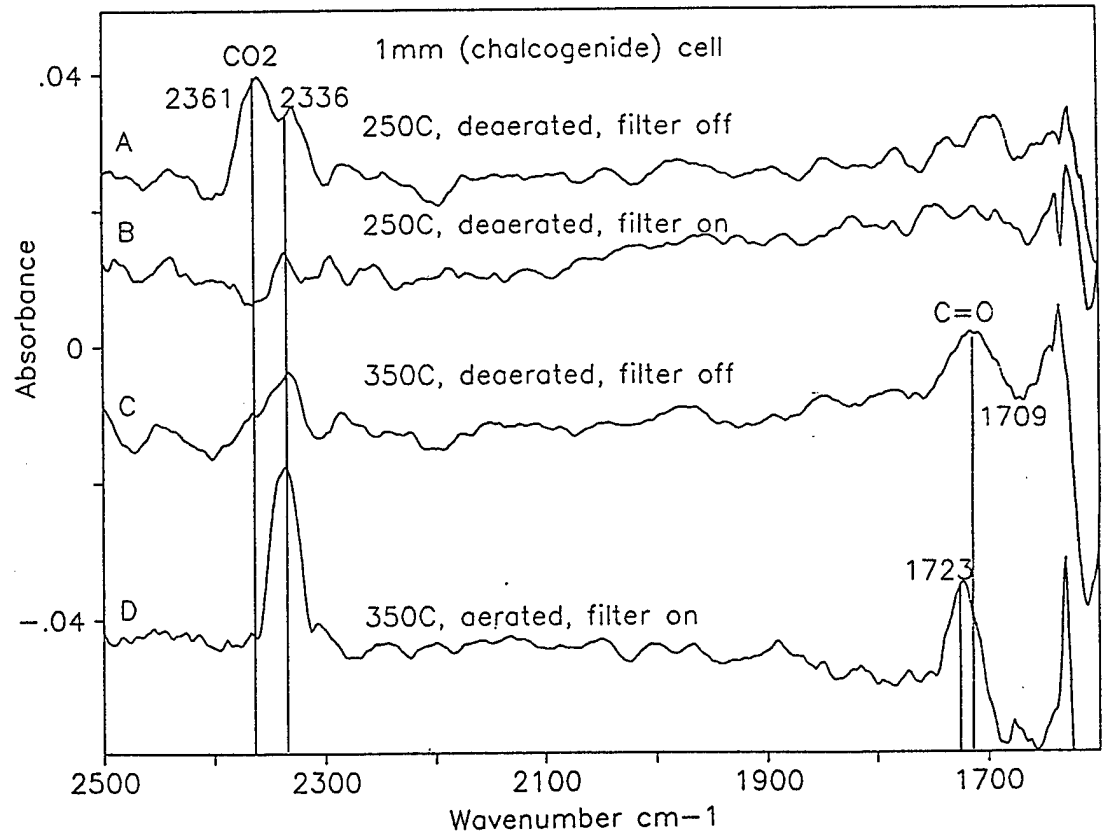

Figure 5.2-2. (a,b,c) Absorbance Spectra Obtained During Thermal Stressing of Deaerated Sun Jet Fuel Showing the Formation of Carbon Dioxide and Carboxylic Acids and d) and Absorbance Spectrum Obtained During Thermal Stressing of an Aerated Sun Jet Fuel Showing the Formation of Carbon Dioxide and Ketones.

Carbonyl formation was also observed for the deaerated fuel, but only at high temperature (Figure 5.2-2c). The position and width of the carbonyl band observed in this case indicates that the product contains a carboxylic acid functionality (1709 cm^{-1}) as opposed to the ketone functionality observed for the aerated fuel at higher wavenumbers (1723 cm^{-1}) (Figure 5.2-2d). The chemistry of carbonyl and CO_2 formation seems to be a general pathway independent of the type of fuel because little difference was observed between the Sun and Shell fuels, as seen in Figs. 5.2-3 and 5.2-4. The sometimes broad carbonyl band is the superposition of "free" carbonyl and carboxyl carbonyl as well as possible hydrogen bonded or other strongly interacting carbonyl species. Figure 5.2-5 depicts a few characteristic shapes of this band observed with the two different fuels at various tempertures and in the presence or absence of the wire probe.

As indicated above, both the CO_2 (around 2300cm^{-1}) and carbonyl (around 1720cm^{-1}) bands occur as two or more overlapping bands which in most cases cannot be easily deconvolved due to the small intensities. However in some cases when significant absorption was observed a deconvolution was possible. The two CO_2 peaks are probably the result of the presence of "free" and "adsorbed" CO_2 with the higher wavenumber species being the adsorbed one. Such a change in band shape and position in the mid-IR is characteristic of a surface-adsorbed species (57). To our knowledge, this behavior has not been previously observed in a stressed fuel system and it must be the result of our high pressure optical cell.

Measurement of Oxidative Stability Using Large Gap Cell - It has been suggested in the literature that the phenomenon of the inverse behavior between thermal and oxidative stability results from the difference in the naturally occurring inhibitor concentrations. Thermally stable fuels usually exhibit low inhibitor concentrations (34,36,39) which in turn facilitates the propagation of oxidation chain reactions. If this is so, the consumption of an inhibitor added to the fuel should be higher with the more stable Sun fuel than the Shell fuel.

In order to test this theory, 250μl of an inhibitor, 4-sec-butyl-2,6-di-tert-butylphenol (SBDTBPH), was injected into the FSTS using an HPLC injector system and its concentration in the fuel was measured as a function of time by monitoring the 3654 cm^{-1} OH stretching band intensity in the 1 mm cell. This is a very sharp peak because no significant interaction of this OH occurs due primarily to steric reasons. Since this band is specific to the presence of the inhibitor, the band intensity is directly related to the inhibiting capacity. Figure 5.2-6 demonstrates how band intensities (relative concentrations) change in the time scale for a particular experiment with aerated and deaerated Sun fuel. One peculiarity is that, at 250 °C, there seems to be a very fast reaction with the fuel but for prolonged times the inhibitor is regenerating. This might mean that an unstable deposit is formed with the inhibitor which slowly decomposes to release the inhibitor back to the system. For most of the experiments, the concentration decrease of the inhibitor exhibited a long tailing, especially at lower temperatures, which could be due to dead volume in the reactor system.

The ratio of the integral of these curves relative to the room temperature integral gives the amount of inhibitor reacted away which is directly related to the natural inhibiting capacity of the fuel at the given temperature and oxygen concentration. Similar experiments were done with the Shell fuel and the results are summarized in Table 5.2-1. The inhibitor consumption is generally significantly higher with the thermally stable Sun fuel, which is consistent with the theory of inverse oxidative and thermal stability (34,36,39).

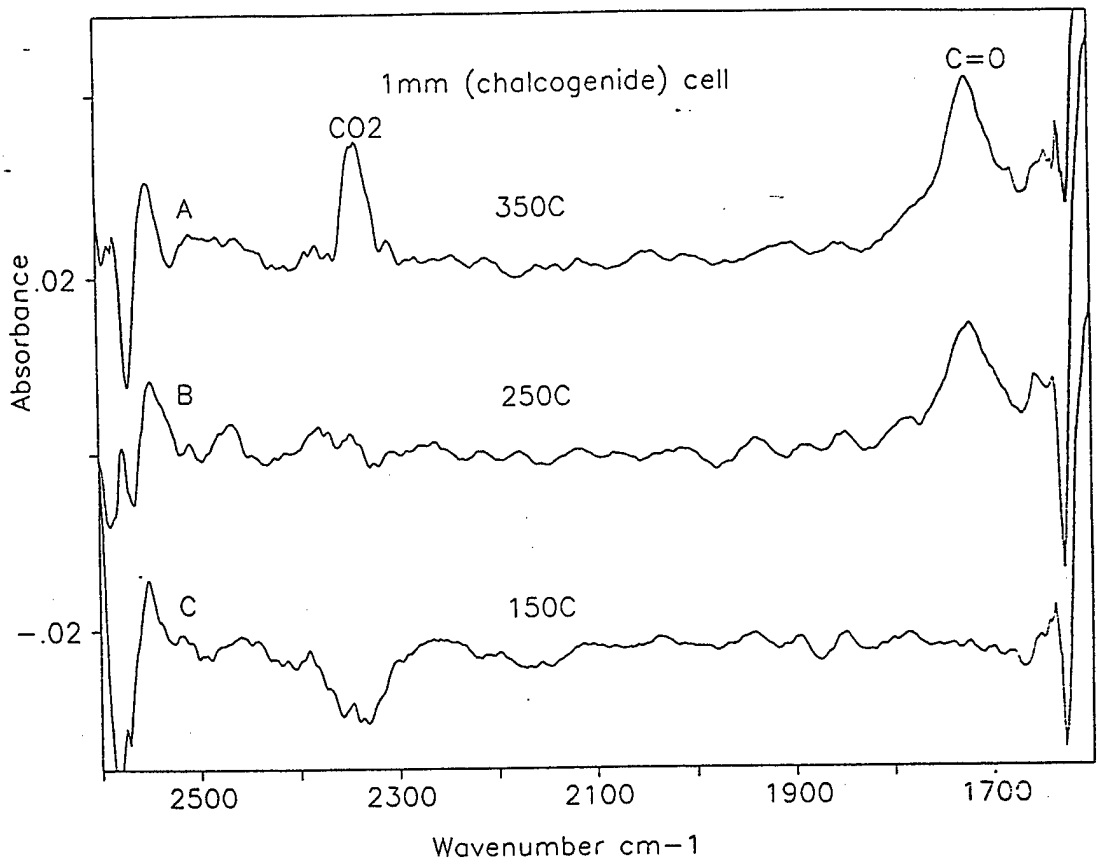

Figure 5.2-3. Spectra from Thermal Stressing of Aerated Shell Fuel Showing Formation of CO_2 and C = O. In Each Case, the Filter Was Off.

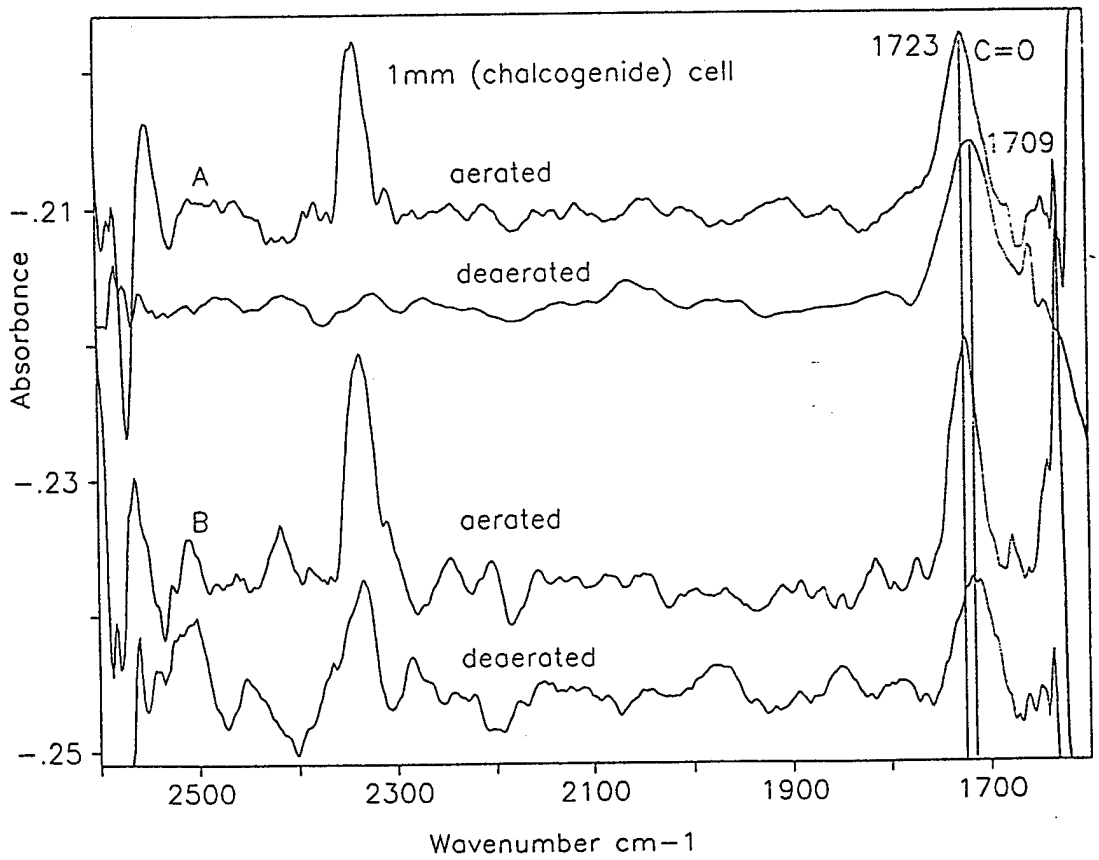

Figure 5.2-4. Comparison of Spectra from Thermal Stressing of Aerated and Deaerated (a) Shell and (b) Sun Fuels. Both Sets of Measurements were Made at 350°C with the Filter Off.

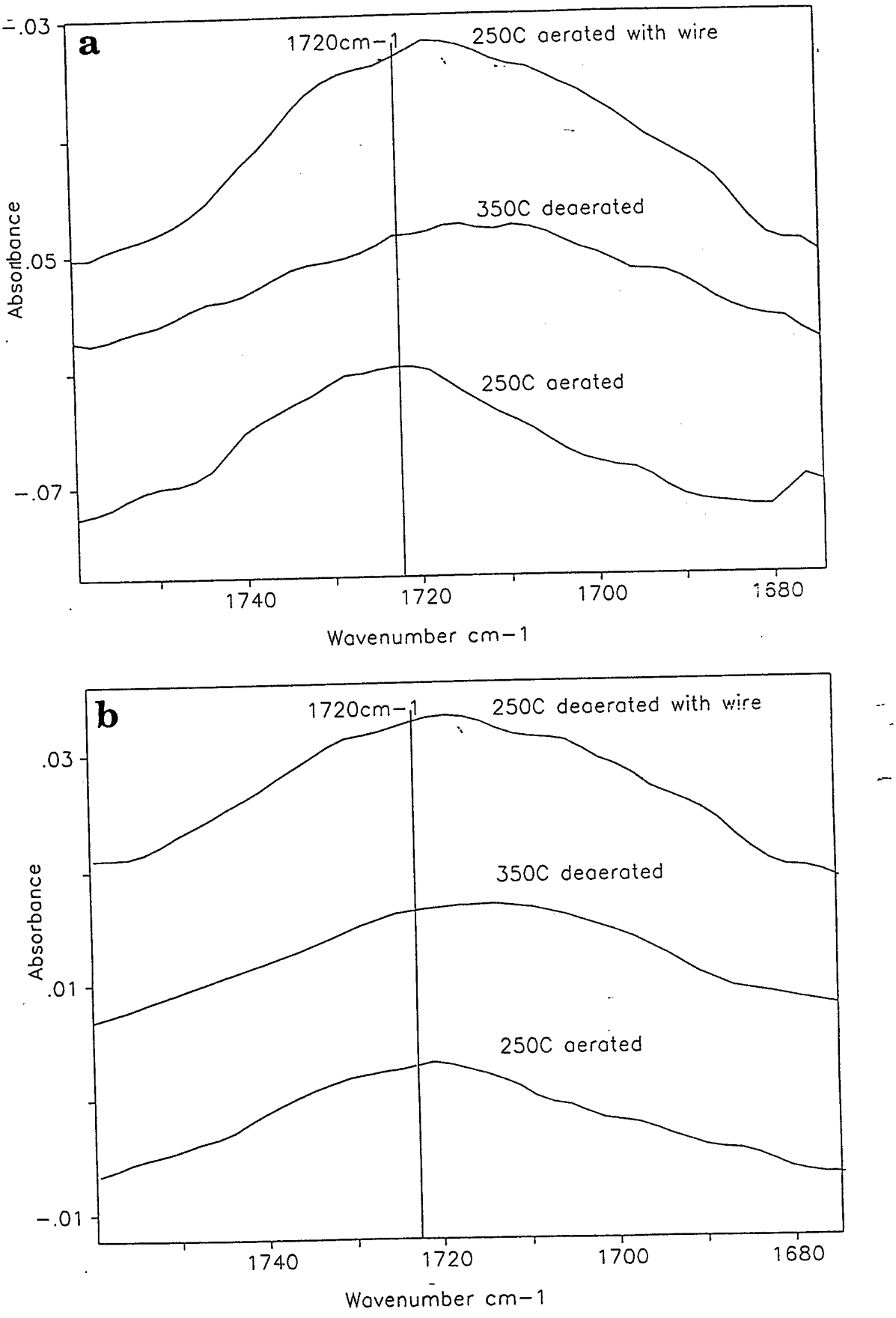

Figure 5.2-5. Dependence of the Carbonyl Band Shape on the Experimental Conditions. a) Sun Fuel; b) Shell Fuel. In Each Case, the Filter was Off.

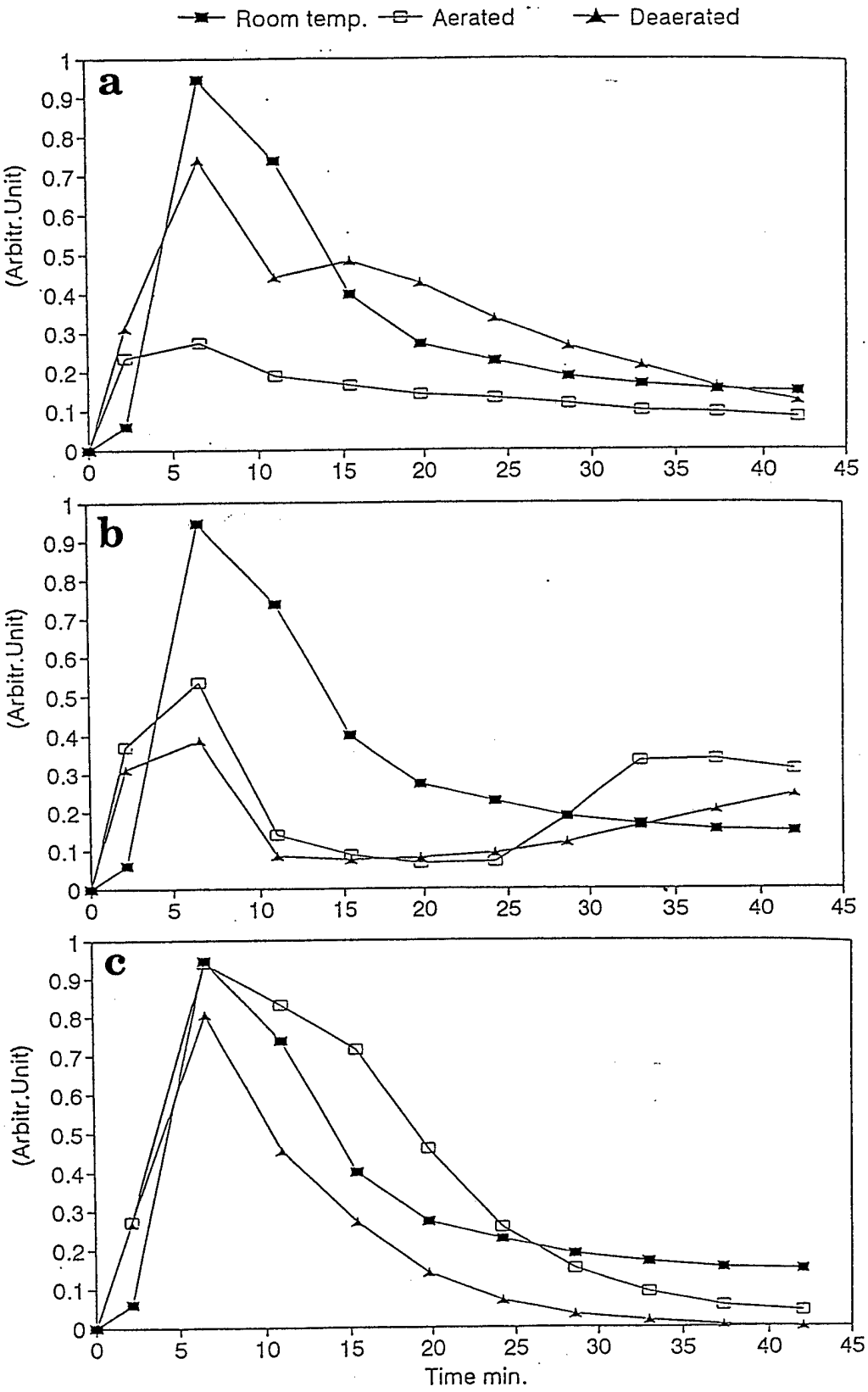

Figure 5.2-6. Change in Inhibitor Concentration with Time for Thermally Stressed Sun Fuel at a) 150°C; b) 250°C; c) 350°C. In Each Case, the Filter was Off.

Table 5.2-1 - Comparison of Inhibitor (SBDTBPH) Consumption in Relative% for Stressed Sun and Shell Fuels.

	Temp. °C	Sun	Shell
Aerated	150	53	0
	250	7	7
	350	6	10
Deaerated	150	0	0
	250	22	7
	350	46	5

In the aerated Sun fuel, the highest reactivity occurs at 150 °C while in the deaerated Sun fuel, the same maximum consumption is shifted to significantly higher temperatures (350 °C).

Since carbonyls are one of the primary products of fuel oxidation, the above-referenced theory of inverse stability would suggest that the amount of carbonyls formed should be higher with a thermally stable fuel than with an unstable one. In order to test this theory, the carbonyl band intensity was calibrated with the acetone carbonyl band intensity based on peak heights and the carbonyl concentrations estimated with the two fuels are summarized in Table 5.2-2.

Table 5.2-2 - Summary of Estimated Carbonyl (C=O) Concentrations (10^{-6} mol/lit) Based on Peak Heights for Thermally Stressed Sun and Shell Fuels

Temp. °C	Sun			Shell		
	Aerated	Deaerated	S(ox)	Aerated	Deaerated	S(ox)
150	0	0		0	0	
250	2	0.9	2.3	1.7	1.7	1
350	2.6	1.3	2	2.1	1.7	1.3

These data indicate that the carbonyl concentrations are slightly higher with the Sun fuel if the fuels contain oxygen. However, this concentration alone is not necessarily a reliable measure of the oxidative stability since the rate of carbonyl formation is also determined by a number of other factors, such as the rate of radical initiation (reaction 1), branching [5-7] and isomerization [10], as indicated by the general free radical scheme for fuel degradation presented under Task 3 (see section 5.3). The reason for the oxidative stability is the presence of inhibitor molecules with weakly bound H-atoms which prevent the radical chain propagation reactions (reaction 3) and instead lead to chain termination reactions [4], thus producing alcohols and carbonyls, as was pointed out by Heneghan and co-workers (34,36,39).

However the reaction

$$R\bullet + AH \rightarrow RH + A\bullet \quad [11]$$

must also be considered. This reaction successfully competes with reaction 2 at low enough oxygen concentrations to transfer the chain to the inhibitor peroxy radical which, by definition, exhibits a significantly lower chain propagation rate and leads to increased radical termination and carbonyl formation.

$$A\bullet + O_2 \rightarrow AO_2\bullet \quad [12]$$

The result is that, with decreasing oxygen concentrations, the carbonyl formation should decrease much less with an oxidatively stable fuel relative to an unstable one. Based on this we suggest the use of S(ox) = aerated/dearated ratio of carbonyl intensities to evaluate the relative oxidative stability. The data in Table 5.2-2 show a significant difference in S(ox) for the two fuels investigated, with the Sun fuel being higher, as expected.

Summary of Measurements of Oxygenated Species with Large Gap Cell - A tabulation of measurements of OH (3250-3700 cm^{-1}), CO_2 (2270-2380 cm^{-1}), and C=O (1680-1760 cm^{-1}) from the large gap cells are given in Tables 5.2-3 and 5.2-4 for the Sun and Shell Fuels, respectively. These results are based on the integrated peak *area* above the integrated noise level according to a method which is outlined below in the discussion of the small gap cell (see equations 1-4). All of these values were normalized relative to the values for the unstressed fuel at the beginning of each experiment, which explains why some of them are negative. This phenomenon was particularly a problem for the OH values, which may be due to contamination of the fuel with moisture. One problem with measurement of oxygenated species is the change in the fuel sample over time. In the Phase II program, we plan to divide the fuel samples into small aliquots at the beginning, which would not be opened until needed for an experiment. If the negative OH values in Tables 5.2-3 and 5.2-4 are not considered, the sum of the oxygenated species (OH+CO_2+C=O) is generally higher for the Sun fuel than the Shell fuel, which is consistent with the other indicators of oxidative stability discussed above, although the carbonyl concentrations based on peak height rather than peak area (see Table 4.4.2-2) show somewhat different trends. Because of the amount of noise in the spectra, the relative concentrations reported in Tables 5.2-3 and 5.2-4 are considered to be more reliable. Selected experiments were done with a more fully deaerated Sun fuel that was produced by storing under vacuum for two days instead of pulling a vacuum and sparging with N_2 for 30 minutes (see Table 5.2-3). As expected, these experiments indicated significantly lower concentrations of oxygenated species.

Under the Phase II program, the cells will be improved to reduce the noise levels, sample handling will be improved to minimize possible contamination, and measurements will be made at much smaller temperature intervals. In the case of the small gap cell, it was found that better temperature resolution revealed important trends that were not previously seen (see discussion of Table 5.2-6).

Summary of Measurements with Small Gap Cell - The IR spectra of the two unstressed fuels collected with the 0.1 mm chalcogenide cell are shown in Fig. 5.2-7. The major regions of absorption are the aliphatic stretching and deformation bands and a small band corresponding to the aromatic ring breathing mode. A previous measurement of the Sun fuel with the same cell (Fig. 5.1-6a) shows some differences due to the change in spectrometers between Task 1 and Task 2. The difference between the two fuels in Fig. 5.2-7 is the higher saturated absorption in the C-H stretching region with the Shell fuel. Because of the saturation problems in the C-H stretching region, the quantitative analyses were carried out with deformation bands, although here possible contributions might occur from phenolic and olefinic functions. Therefore an improved cell would have a smaller (around 0.05 mm) gap between the two ends of the fibers. This would require the

Table 5.2-3 - Measurements of Oxygenated Species for Sun Fuel with the Large Gap Cell (relative to unstressed fuel)

Fuel	Temp. °C.	Absorption band intensities (peak area)				Arbitrary units	
		OH	St. Dev.	CO_2	St.dev.	C=O	St.dev.
Sun							
aerated	150	0.76	0.65	0.38	0.06	-0.26	0.04
	250	4.40	0.55	0.00	0.02	0.30	0.01
	350	0.30	0.56	0.33	0.02	0.12	0.02
	450	-5.81	2.43	-0.33	0.05	0.34	0.03
Sun							
deaer (a)	150	-0.34	0.60	0.06	0.02	0.09	0.02
	250	-0.63	0.64	0.43	0.02	0.24	0.02
	350	-0.40	0.63	0.16	0.03	0.38	0.02
Sun							
deaer (b)	150	-2.75	2.53	0.13	0.05	0.00	0.04
	250	-1.44	2.12	0.03	0.05	0.11	0.03
	350	1.55	2.02	0.11	0.05	0.23	0.04

a: partially dearated
b: completely deaerated

Table 5.2-4 - Measurements of Oxygenated Species for Shell Fuel with the Large Gap Cell (relative to unstressed fuel)

Fuel	Temp. °C.	Absorption band intensities (peak area)				Arbitrary units	
		OH	St. Dev.	CO_2	St.dev.	C=O	St.dev.
Shell							
aerated	150	-0.06	0.51	-0.15	0.02	0.02	0.01
	250	0.6	0.45	0.11	0.02	0.43	0.01
	350	1.01	0.53	0.27	0.02	0.58	0.02
	450	*25.21	3.24	0.02	0.07	0.47	0.05
Shell							
deaerated	150	-0.23	0.22	0.08	0.01	0.07	0.01
	250	0.13	0.25	-0.02	0.03	0.26	0.02
	350	0.04	0.28	0.11	0.02	0.27	0.02

*: probable water contamination

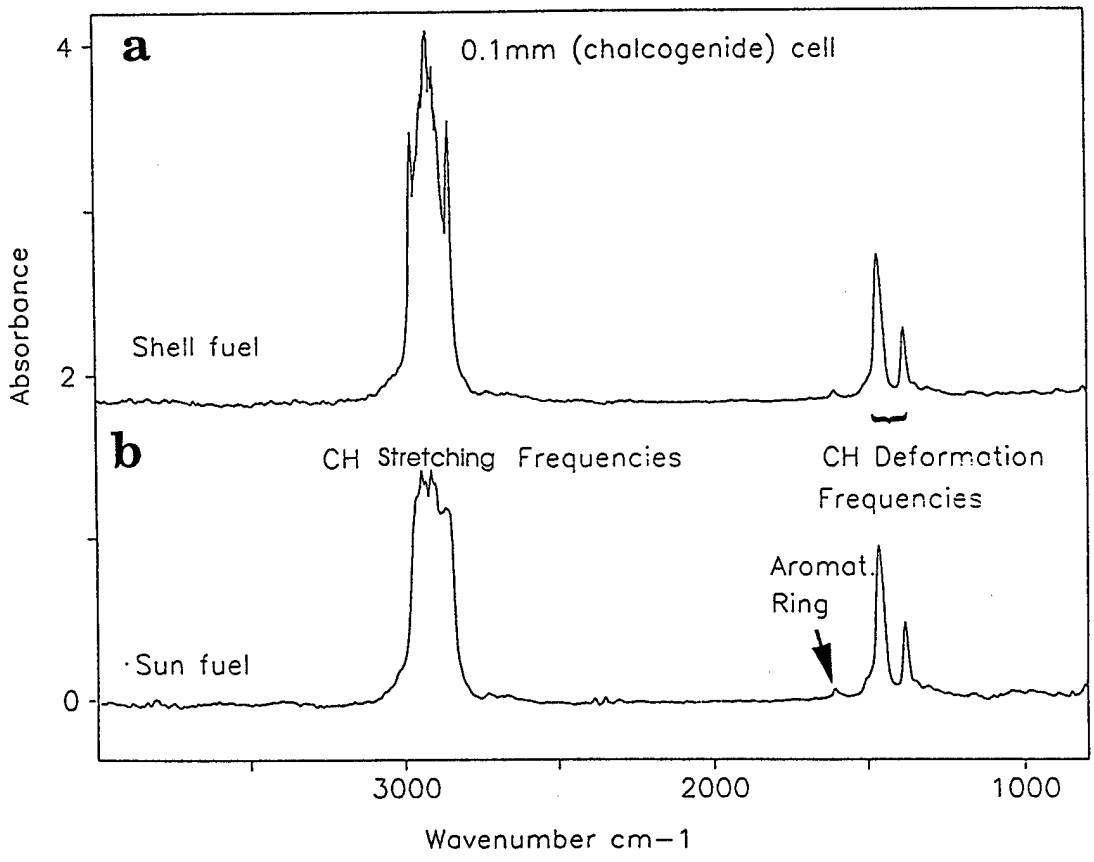

Figure 5.2-7. Comparison of IR Spectra of Unstressed Shell and Sun Fuels from 0.1 mm Cell.

manufacture of more precisely polished and positioned fibers, which will be done under Phase II (42). The sensitivity of the small gap cell as applied for the particular purpose of testing fuel degradation was tested in the following ways. 1) a 2 micron filter was introduced between the reactor and the cell; 2) a stainless steel wire was introduced into the reactor. FT-IR difference spectra were determined for both cases over a wide range of conditions, which indicated that these measurements in the small gap cell were very sensitive to changes in fuel composition due to degradation or filtration for both fuels.

The initial experiments were designed to gain insight about the formation of insoluble materials during thermal stressing as a function of oxygen content in the fuel. Aerated and deaerated Sun and Shell jet fuels were stressed and spectra were collected at 150 °C, 250°C, and 350°C in both the "filter off" and "filter on" modes. The absorbance spectra obtained at each temperature for the "filter on" case were subtracted from the corresponding spectra for the "filter off" case after both were ratioed to the unstressed fuel. The positive bands observed in these difference spectra represent the material removed from the stressed fuel by the filter. Negative bands were also observed in the difference spectra, and are tentatively assigned to the fuel that fills the "voids" resulting from the removal of insoluble material. This interpretation is consistent with the effects observed for the doped fuels discussed under Task 1 (see Section 5.1, Figs. 5.1-7 to 5.1-9); although other explanations are possible. To the extent that the deposits are similar to the bulk fuel, these effects would tend to cancel each other and no net change would be observed. In the case where the deposits are significantly different in composition than the bulk fuel (which is more likely), both positive and negative peaks would be observed. Consequently, there is a theoretical basis for quantifying the absolute value of the changes in the difference spectra as an indicator of deposit formation tendencies.

The initial experiments indicated significantly larger peaks in the difference spectra for the aerated Shell fuel vs the Sun fuel, as expected from the known differences in thermal stability. However, a problem was observed in repeating the measurements which were originally done in two parallel experiments under the same conditions, one set with the filter on and one set with the filter off. The problem was traced to leakage in the small gap cell that led to an unstable signal under the same nominal conditions. The problem was corrected and the measurements were repeated.

The results for the difference spectra are shown in Figs. 5.2-8 and 5.2-9 for experiments in the absence and presence of a steel wire, respectively. In order to increase the signal to noise ratio, two times one hundred interferograms (double buffer mode) were coadded and two to five absorption spectra were averaged. Since the spectra were referenced to the "untreated" fuel itself they truly represent the changes that occur as a result of a particular treatment (filter switch and/or thermal stressing).

As a result of saturation, the 3000-2700cm^{-1} region can not be seen although, as discussed above, this would be the most sensitive area for the measurements. This calls for a smaller gap cell which we plan to manufacture using precise optical gaping technology under Phase II (42).
The other important region is the aliphatic deformation region around 1400 cm^{-1}. As it can be seen in Figs. 5.2-8 and 5.2-9, there was a response to changing experimental conditions (filter switch, thermal stress or the presence of the wire probe) in this region -both positive and negative.

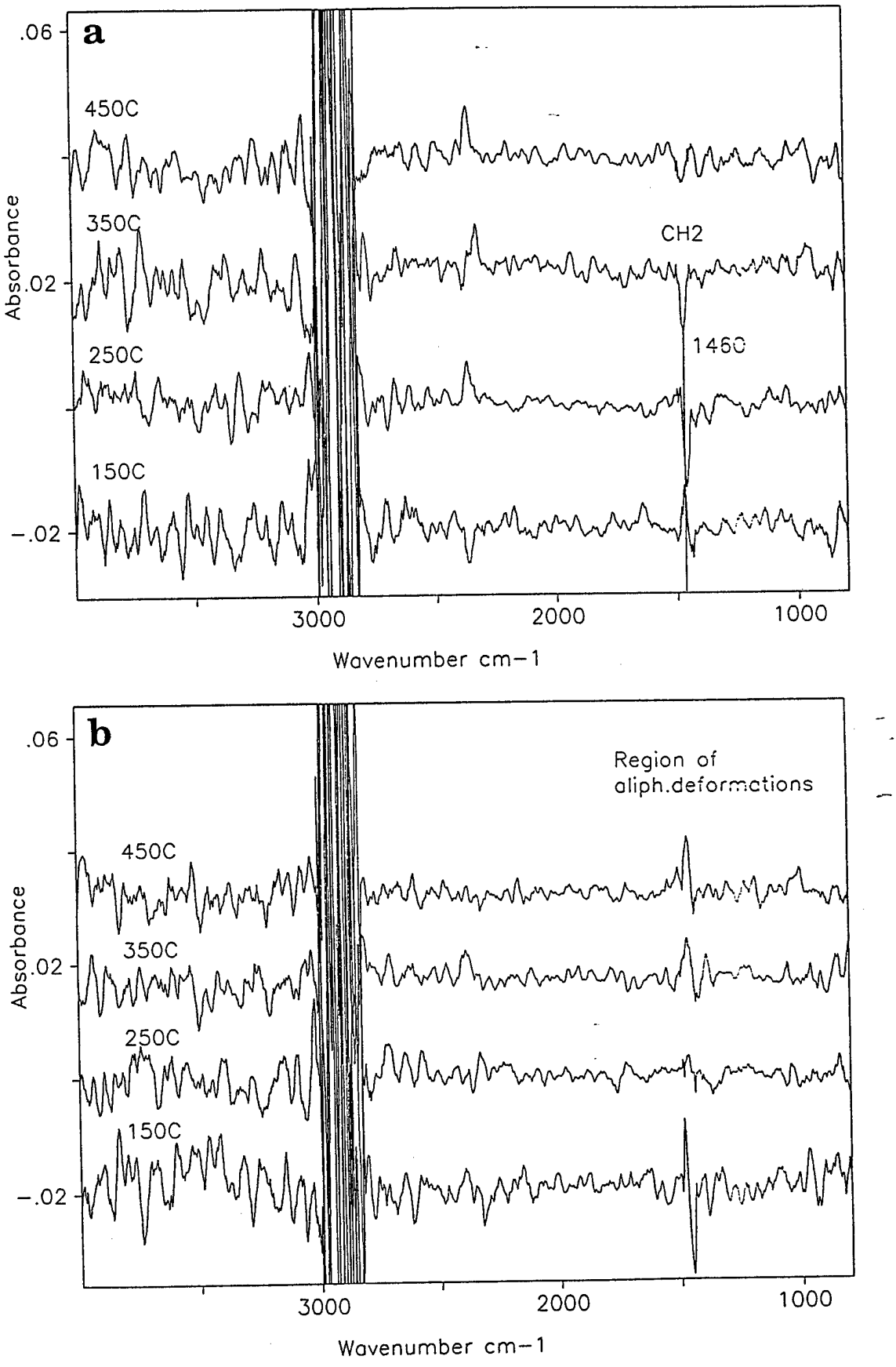

Figure 5.2-8. Difference (filter off-on) Spectra with Stabilized Small Gap Cell for a) Aerated Sun Fuel and b) Aerated Shell Fuel Stressed without the Steel Wire Present.

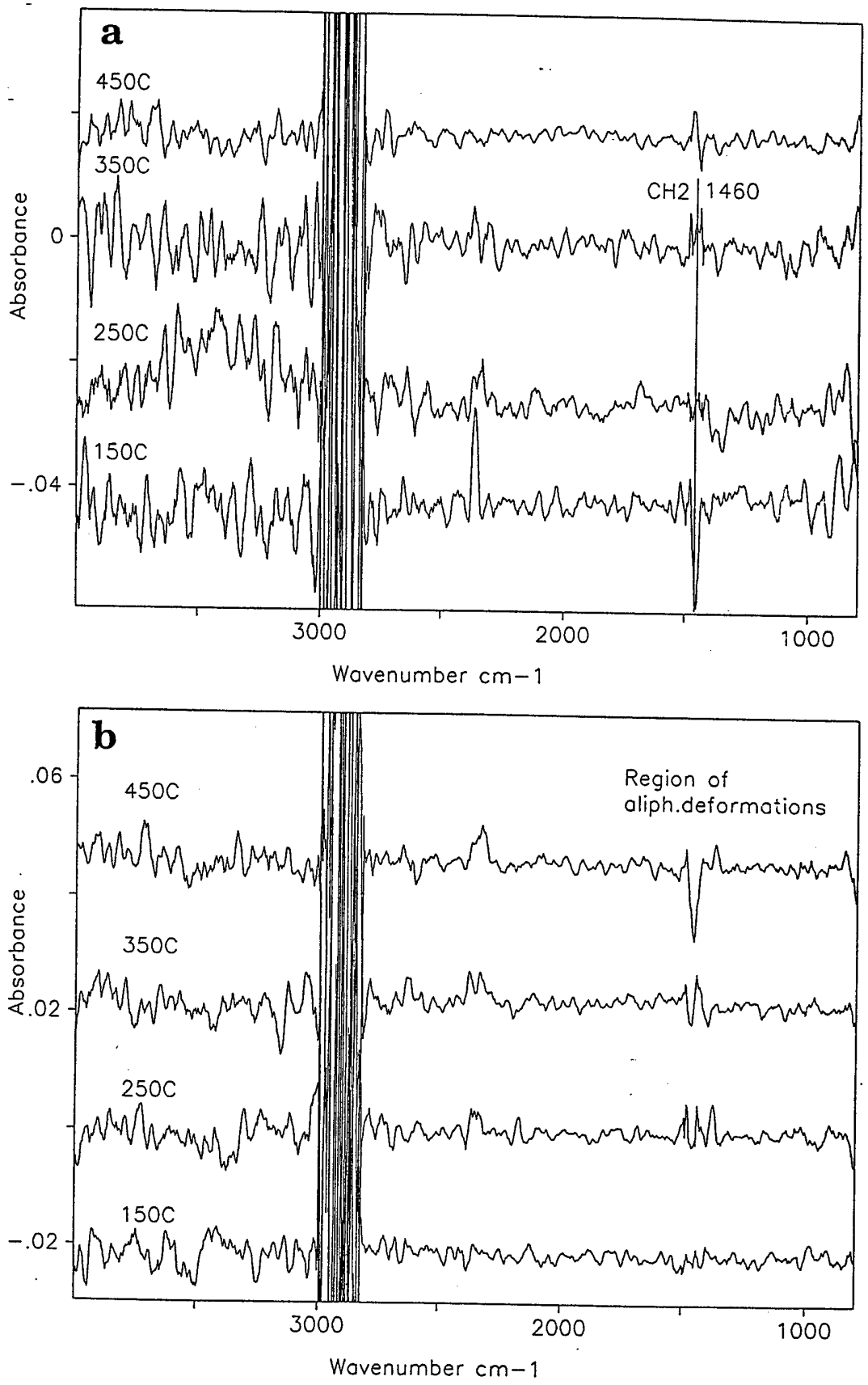

Figure 5.2-9. Difference (filter off-on) Spectra with Stabilized Small Gap Cell for a) Aerated Sun Fuel and b) Aerated Shell Fuel Stressed in the Presence of a Steel Wire.

The observed spectral responses to thermal treatments were generally very small, both for the aliphatic deformations as measured with the small gap cell and for the oxygenates measured with the large gap cell (discussed previously). Because of the small signal to noise ratio, peak areas were used instead of the usual peak heights and the data for the experiments done in the absence of the wire probe are summarized in Table 5.2-5. The absorption intensities were calculated as

$$A(absorption)=\sum_{y=L}^{y=u}(I(x,y)-NS) \qquad (1)$$

Here I(x,y) is the intensity of absorption x at a particular wavelength y and the summation is carried out between the lower (l) and upper (u) limit of the spectral envelope (l,u) containing the particular absorption mode. N is the number of points in the envelope (l,u) or the resolution and S is the standard deviation of the noise for a wider spectral range (lw,uw) in the vicinity of envelope (l,u)

$$S=3\frac{\sqrt{\sum_{y=Lw}^{y=uw}(I(x,y))^2}}{Nw} \qquad (2)$$

where lw and uw are the lower and upper limit and Nw is the number of points respectively for the (lw,uw) envelope of a particular spectra. The standard deviations as shown in Tables 5.2-3 to 5.2-6 are NS (S multiplied by the number of spectral points in the particular (l,u) envelope) in order to quantify the characteristic noise relative to the signal.

As discussed above, the small gap transmission cell data show both negative and positive features in the aliphatic deformation region for the difference spectra. Because these might be characteristic of both the fuel and the degradation process, it was decided to use absolute values in order to determine the spectral "response" or "perturbation".

$$A'(absorpt.)=Resp.(absorpt)=ABS\sum_{y=L}^{y=u}((ABS(I(x,y)-B)-NS) \qquad (3)$$

where B is the spectral average or corrected baseline as calculated for the wider spectral range.

$$B=\frac{\sum_{y=Lw}^{y=uw}I(x,y)}{Nw} \qquad (4)$$

Since A(absorpt.)=Resp.(absorpt.) is the superposition of both positive and negative spectral changes, it was called the Response factor or Resp.(absorpt) rather than absorption. The correction with B is necessary to compensate for sample to sample baseline shifts. Baseline shifts occur as a result of IR source (globar) variations, mirror switching, cell positioning and other instabilities.

Table 5.2-5 IR Spectral Response Data for Aliphatic Deformation Region for the Small Gap Cell

	Temp. °C.	IR spectral Response [a]	St. Dev.	Ratio* CH_2/CH_3	Diff. spectral Response [b]	St.dev.	Ratio* CH_2/CH_3
Reference				0.16	0.04		
Sun							
no wire	150	0.30	0.07	0.88	0.18	0.06	0.99
aerated	250	0.61	0.07	0.80	0.31	0.04	0.84
	350	0.28	0.09	0.97	0.23	0.06	0.82
	450	1.26	0.15	0.75	0.19	0.04	0.85
Shell							
no wire	150	0.46	0.06	0.86	0.41	0.07	0.87
aerated	250	0.59	0.07	0.72	0.18	0.05	0.76
	350	0.46	0.07	0.75	0.20	0.05	0.78
	450	0.32	0.08	0.80	0.19	0.05	0.89

Table 5.2-6 Additional IR Spectral Response Data from Aliphatic Deformation Region for Aerated Shell Fuel

	Temp. ° C.	IR spectral Response [a]	St. Dev.	Ratio* CH_2/CH_3	Diff. spectral Response [b]	St.dev.	Ratio* CH_2/CH_3
Reference					0.16	0.04	
Shell	150	0.46	0.06	0.86	0.41	0.07	0.87
no wire	250	0.59	0.07	0.72	0.18	0.05	0.76
	350	0.46	0.07	0.75	0.20	0.05	0.78
	375	0.42	0.08	0.83	0.53	0.08	0.82
	400	0.39	0.11	0.84	0.34	0.08	0.82
	425	0.54	0.14	0.78	0.38	0.07	0.84
	450	0.32	0.08	0.80	0.19	0.05	0.89
	475	0.64	0.15	0.70	0.35	0.08	0.81
	500	0.95	0.17	0.74	0.50	0.08	0.86

Notes for Tables 5.2-5 and 5.2-6
*: Ratio= $CH_2/(CH_2+CH_3)$

a: measured relative to unstressed fuel, filter off

b: difference of IR Spectral response for the filter off-filter on cases

The CH_2/CH_3 ratio, which was shown in a previous Phase I SBIR project (28,29) as characteristic of the deposit formed on the surface of the ATR fiber is difficult to express quantitatively for the bulk fuel because of the small signal intensities. However an approximation was made using the (1505,1405 cm^{-1}) and (1405,1340 cm^{-1}) envelopes to calculate the CH_2 and CH_3 intensities respectively and the ratio is expressed as $CH_2/(CH_2+CH_3)$.

The summary of both the absolute (filter off) and differential (filter off-filter-on) response factors and the ratios in Table 5.2-5 did not appear to show any clear trends. However, it has been observed in the literature that the deposit formation in relatively stable jet fuels exhibits a sharp maximum at about 370 °C (36). With this in mind, we tested the sensitivity of our small gap cell towards this phenomena using the remaining supply of Shell fuel (the Sun fuel had been depleted). Since the maximum seems to be very sharp, we collected the filter on and off spectra in 25 °C steps above 350 °C up to 500 °C. The sharp increase of pressure above 500 °C did not allow the system to be tested at much higher temperatures. The results are summarized in Table 5.2-6. and Fig. 5.2-10. As it can be seen the Response Factors as calculated from the difference (filter off - filter on) spectra parallel the literature findings for a similar fuel stressed under similar condtions (Fig.5.2-11). These results suggest that the small gap cell-filter system is an appropriate tool for fast, precise and reliable testing of deposit formation in jet fuels both at low (150 °C) and high temperatures. Of course, these measurements will need to be repeated for a variety of fuels, as is planned for Phase II, Task 2. It should be emphasized here that the 500 °C upper limit was not limited by the IR cells but the present set up of the system. An appropriate higher back pressure regulator will allow this temperature limit to be raised significantly.

The interesting feature of the data is that the absolute spectral response of the thermal stressing of the fuel (solid symbols in Fig. 5.2-10a) does not follow the filter response or the deposit maximum, which indicates that the filter response is a unique and simple way of testing these fuels.

Another observation is that the $CH_2/(CH_2+CH_3)$ ratio, as measured for the bulk (unfiltered) fuel, also shows a maximum in this temperature region whereas this ratio calculated from the difference spectra does not (See Figure 5.2-10b). Although it is hard to explain this phenomenon based on our present knowledge of the behaviour of the fuels at these temperatures, it suggests that the maximum is more likely a result of fuel chemistry effects and not from hydrodynamic or other effects, the same conclusion that Edwards and Zabarnick reached (36).

Summary of Effects of Wire Probe on Fuel Degradation - The use of a wire probe to collect deposits in the thermal stressing reactor had an unintended effect of changing the course of the thermal degradation. This can be clearly observed in Table 5.2-7 in the changes in the amount of soluble gum formed. The rest of the data in this table are uninteresting because of the small amounts of deposits that could be recovered from the cold filter or hot wire. The same collection methodology had been successfully used in a previous program which had a significantly larger reactor zone and longer reaction times (fuel volume) per measurement (18). The presence of the wire also had a dramatic effect on the amounts of CO_2 and C_2O formed for the Shell fuel but not for the Sun fuel. The reverse was true of the OH concentrations. The effects of the wire probe can also be clearly seen in the spectral data from both the small and large gap cell. Figures 5.2-12 and 5.2-13 show the absolute spectral response (filter off) for the Sun and Shell fuels respectively and how this changes with the wire present. These changes are less evident with the difference spectra (compare Figs. 5.2-8 and 5.2-9). Effects of the wire probe can also be seen data for the carbonyl region from the large gap cell in Fig. 5.2-5. The fact that significant changes could be seen in data from both cells and in the amounts of gums formed supports the idea that the IR measurements are very sensitive to changes in the fuel properties and that it should ultimately be possible to correlate these measurements. This result is also consistent with earlier

Table 5.2-7 - Off-line Measurements of Filter Deposits, Wire Deposits, and Soluble Gums from Aerated Sun and Shell Fuels Stressed to Various Temperatures

Temp °C	Fuel	weight % x 10^2			
		Deposits		Soluble Gum	
Room	Sun	Filter	Wire	no Wire 0.83	with Wire
150		0	0.05	1.62	0.38
250		0	0	1.76	0.61
350		0.13	0	0.64	0.86
450		0.09	0	0.47	0.53
Room	Shell			6.41	
150		0.02	0	3.86	0.83
250		0.1	0	1.02	1.68
350		0	0	4.46	1.45
450		0.07	0	2.03	0.93

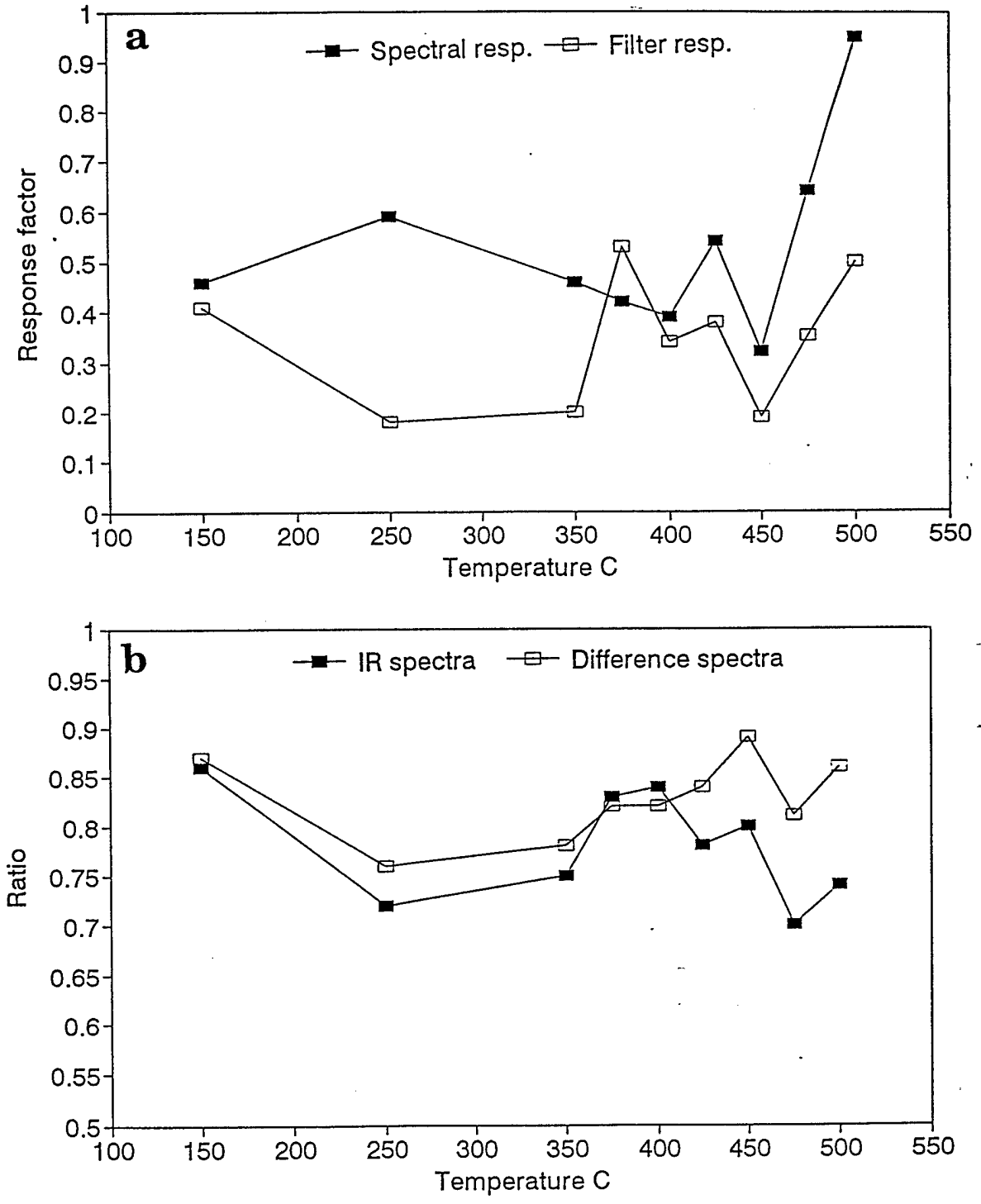

Figure 5.2-10. Results from Small Gap Cell and C-H Deformation Region for Thermal Stressing Experiments with Aerated Shell Fuel. a) Absolute Response (closed symbols) and Differential Spectral Response (filter off - filter on)(open symbols); b) $CH_2/(CH_2 + CH_3)$ Ratio Determined from the Absolute Spectral Response (closed symbols) or the Differential Spectral Response (filter off - filter on)(open symbols).

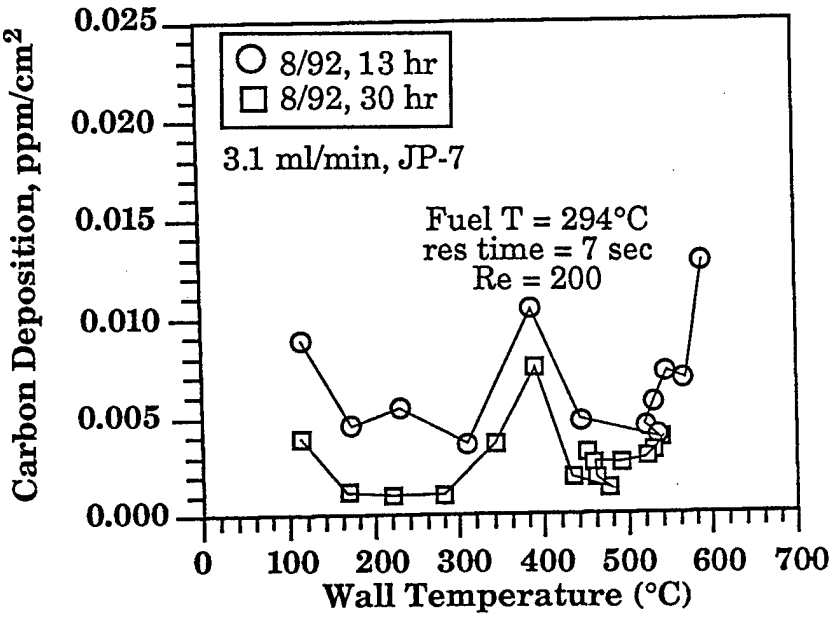

Figure 5.2-11. Results from 3.1 mL/min Tests. Air Sparged JP-7 Fuel, 69 atm. Data of Edwards and Zarbarnick, Ind. Eng. Chem. Res., **32**, 3117 (1993).

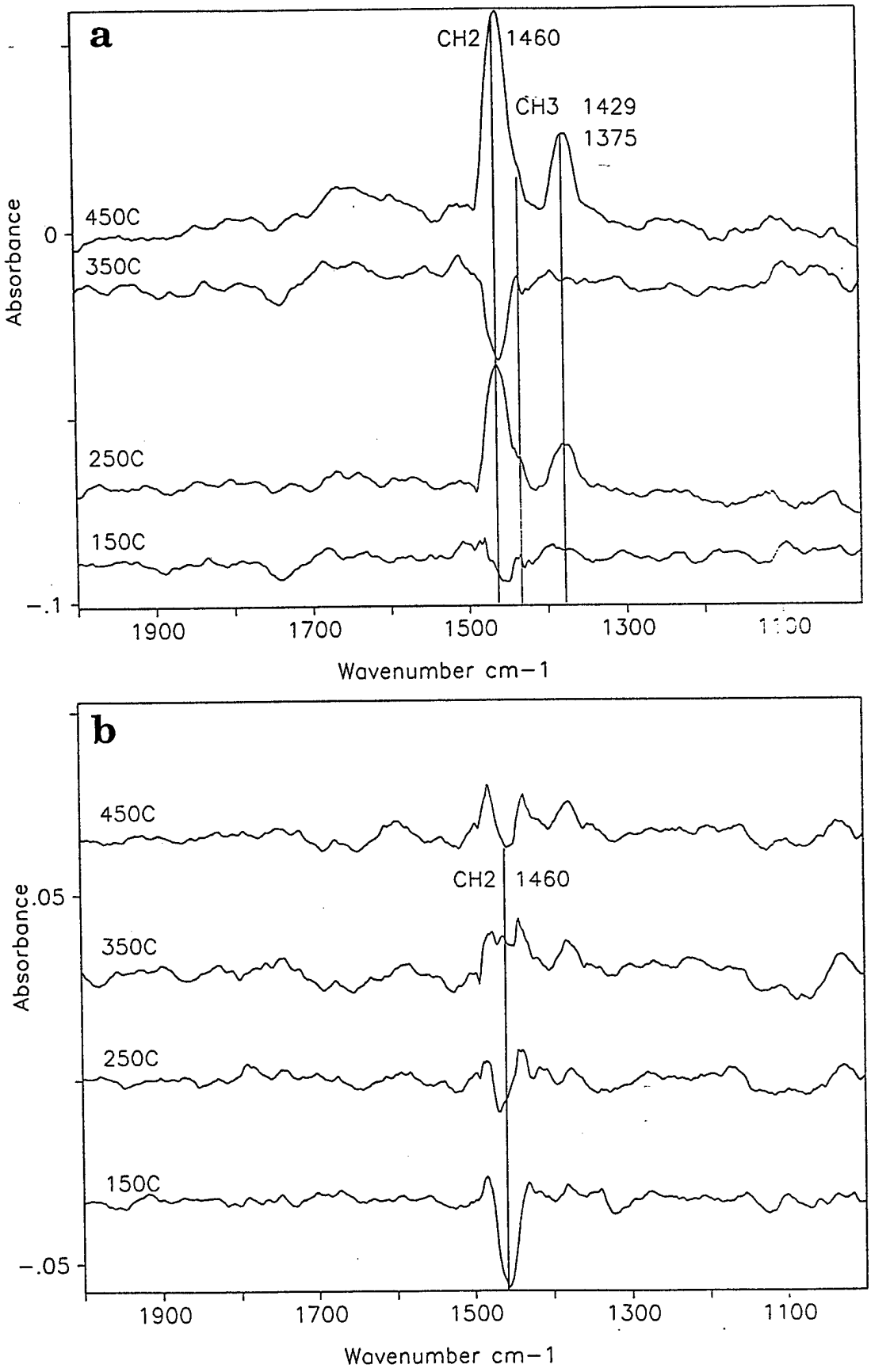

Figure 5.2-12. Absorption Spectra Referenced to the Unstressed Fuel for Aerated Sun Fuel a) Without Wire in the Reactor and b) With Wire in the Reactor.

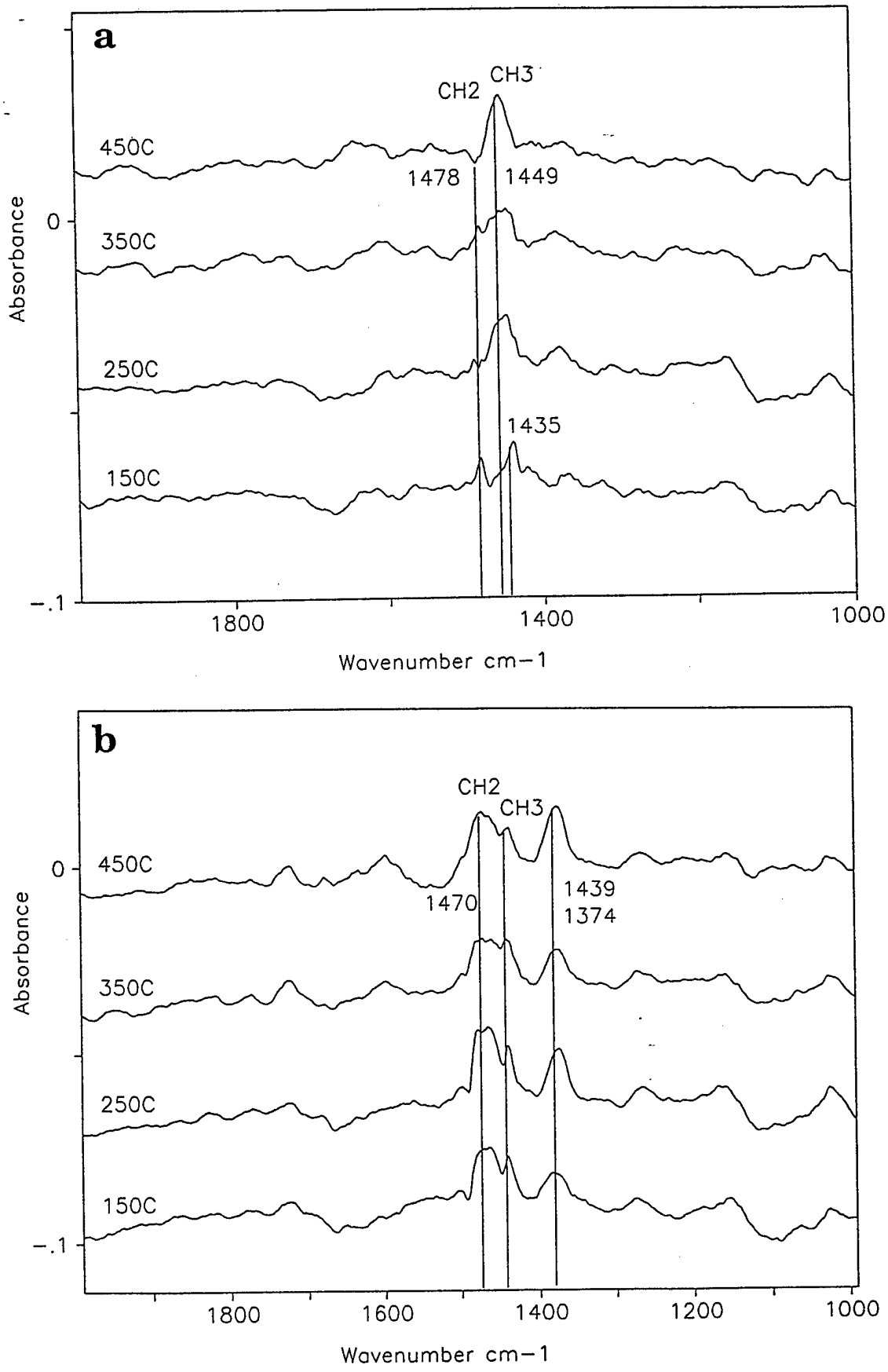

Figure 5.2-13. Absorption Spectra Referenced to the Unstressed Fuel for Aerated Shell Fuel a) Without Wire in the Reactor and b) With Wire in the Reactor.

work at AFR which indicated a correlation between gum formation and an increased olefin absorbance measured in the IR (17,18).

Field Ionization Mass Spectrometry (FIMS) of Wire Deposits - Samples of the wires from experiments with both fuels were sent to SRI International (Menlo Park, CA) for analysis by FIMS. In this case, pieces of the wire were cut, placed in the inlet probe of the mass spectrometer and then heated at about 3 °C/min to ~ 500 °C. Results of four of the five samples that were analyzed are shown in Fig. 5.2.14. A fifth sample from Sun fuel (150 °C, aerated) was similar to Fig. 5.2-14d and is not shown. In both samples of wires from experiments with the Sun fuel, there was essentially no deposit formation, and the peaks that were found were probably derived from additives in the fuel. The high thermal stability of the Sun fuel toward deposit formation is consistent with its higher JFTOT breakpoint temperature (332 °C vs. 263 °C for Shell). These results are also consistent with the relatively small amount of deposit formation for the Sun fuel and large amount for the Shell fuel on a fiber optic attenuated total reflectance (ATR) probe investigated in a previous program (28,29) and the relatively high oxidative instability of the Sun fuel when compared to the Shell fuel observed in the current program.

In the case of the Shell fuel, the FIMS spectra are more complex than observed previously for the JP-5 fuel (17,18), which appeared to be dominated by a series of aliphatic waxes. The fiber optic ATR spectra for the Shell fuel, also supported the characterization of the deposits as of aliphatic character, although the sapphire fiber used cut off the part of the mid-IR spectra that is most sensitive to aromatic and oxygenated species formation (28,29). This may explain the more complex nature of the deposits observed in the case of the Shell fuel, where the aliphatic series of peaks is still present but not dominant. It is not surprising that the deposit composition would also depend on the fuel composition, since the precursors and solubility characteristics are different for each fuel. It should also be noted that the aliphatic nature of the JP-5 deposits may be less than what a casual examination of the FIMS spectra would suggest. This is because a carbonyl group would add the same number of mass units as 2 aliphatic $-CH_2-$ groups. Consequently, it would be more correct to revise our original statement to say that deposits from the JP-5 fuel appear to consist of aliphatic waxes and aliphatic carbonyls. This is consistent with the FT-IR spectra of these deposits which show a strong carbonyl band (17,18), as well as the statement by Heneghan and Zabarnick that deposits produced according to the accepted free radical mechanism (see Task 3) should be rich in heteroatoms (39).

Summary of Task 2 - In-situ IR transmission measurements were made of peroxide decomposition products from stressed fuels including carbonyls (free and acid form), alcohols, and CO_2 (two forms). The measurements of CO_2 are believed to be the first reported measurements in a stressed jet fuel. It was demonstrated that the IR transmission measurements are consistent with the generally accepted free radical mechanism of fuel degradation, including the inverse relationship between oxidative and thermal stability. A methodology was also demonstrated for predicting the deposit forming tendencies by the perturbations of FT-IR transmission measurements when an in-line filter is used, which agrees well with results from the literature. It was found that both the large gap (1 mm) and small gap (0.1 mm) IR transmission measurements were very sensitive to the presence of a steel wire probe in the quartz lined thermal stressing reactor, which was consistent with significant changes in the soluble gum formation that were observed with the wire present.

5.3. Task 3 - Data Interpretation and Modeling

Objective

Data developed in Task 2 will be analyzed along with existing data and models in order to develop

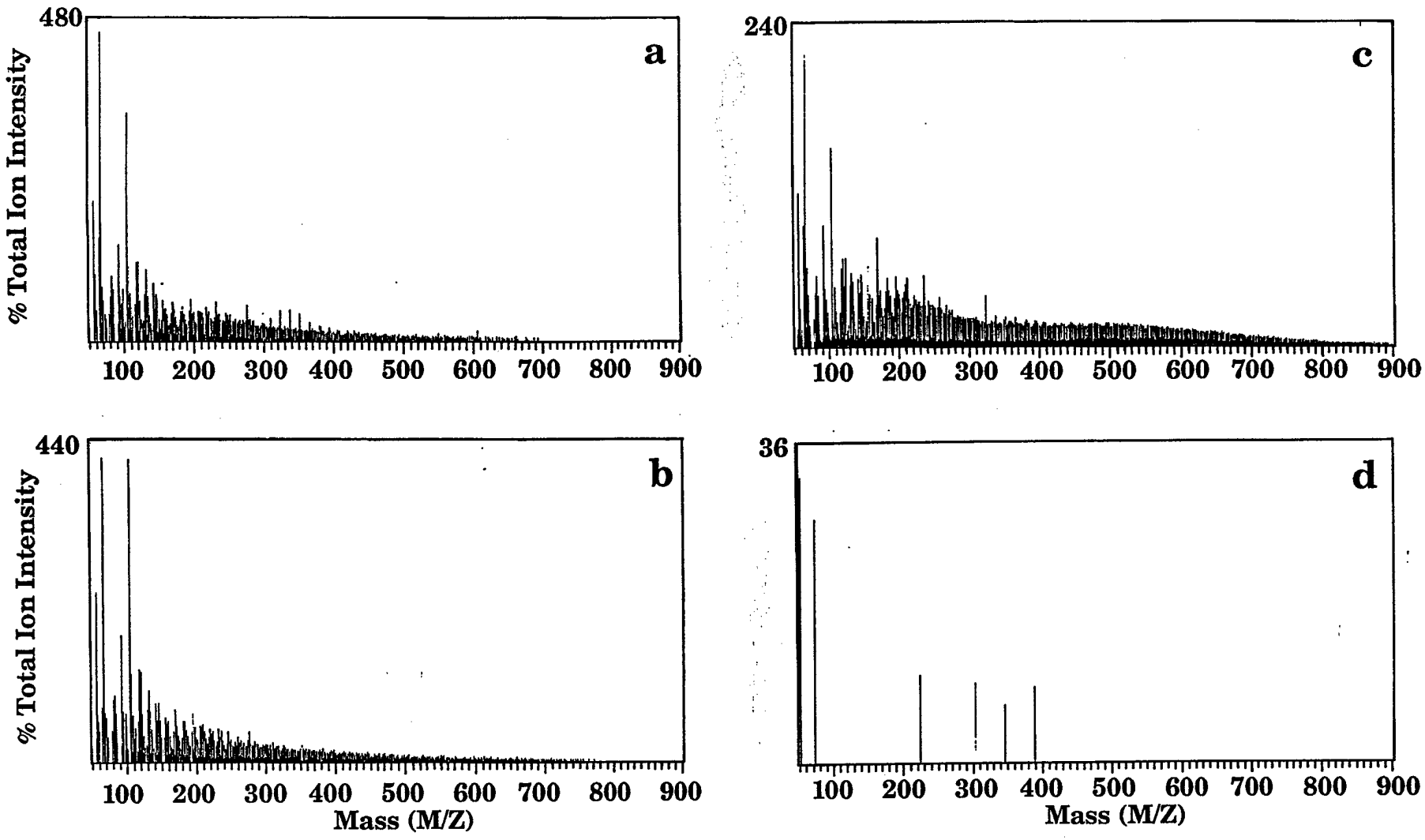

Figure 5.2-14. Field Ionization Mass Spectra of Wire Deposits from Shell and Sun Fuels. a) Shell 150°C, Aerated; b) Shell 150°C, Dearated; c) Shell 350°C, Aerated; and d) Sun 350°C, Aerated.

a quantitative model that can describe fuel degradation at temperatures up to 400 °C. The model would be formulated under the Phase I program but would not be extensively tested until Phase II.

Methodology

Mechanistic Modeling - In our mechanistic modeling effort we wish to identify chemically significant reactions leading to gums (soluble and insoluble) and deposits. We will start with a general scheme for the oxidation and thermal decomposition of hydrocarbons including all the relevant oxygenated intermediates. For this purpose, we plan to expand the model of Zabarnick (35) and extend it to higher temperatures. This work will be done under the Phase II program.

Global Modeling - Global reaction modeling is essential for translating data obtained on a laboratory scale into a form than can be used for design and/or performance of real systems. A good global reaction model should have the following characteristics: 1) it must be accurate over the entire range of each operating parameter; 2) it must be applicable to systems of different geometry; and 3) it must usually be justified physically and chemically. AFR's experience has been in developing global models for coal devolatilization that are based on the functional group distributions and weak bond linkages within the coals and which have been quite successful at reproducing and predicting pyrolysis yields over a wide range of coal rank and polymer systems as discussed in Refs. 58 and 59.

In the previous work, a global three step kinetic model was developed to describe the deposit formation under various fuel stressing conditions (17,19). This model also incorporated mass transfer effects. The major modeling effort was focused on explaining the lower deposit formation at high temperatures by the presence of significant mass transfer resistances and the decomposition of the oxidative precursor. Incorporation of mass transfer also enables the influence of flow rate on deposit formation to be explained. The AFR model was successful in modeling the UTRC data published by Giovanetti and Szetela (30).

Work Performed

Data Interpretation - The results discussed Under Task 2, above, are consistent with the generally accepted mechanism for fuel degradation in the presence of oxygen via the branching chain reaction involving hydroperoxide radicals (39-41):

Chain initiation:	$RH \rightarrow R\bullet + H\bullet$ (slow)	[1]
Propagation:	$R\bullet + O_2 \rightarrow ROO\bullet$	[2]
	$ROO\bullet + R'H \rightarrow ROOH + R\bullet$	[3]
Termination:	$ROO\bullet + R'OO\bullet \rightarrow ROH + R'{=}O + O_2$	[4]
Branching:	$ROOH \rightarrow RO\bullet + OH\bullet$	[5]
	$RO\bullet + R'H \rightarrow ROH + R'\bullet$	[6]
	$OH\bullet + RH \rightarrow HOH + R\bullet$	[7]

Additionally, the possibility of the following radical isomerization reactions has also been suggested by Edwards and Zabarnick (36):

$RO\bullet \rightarrow R'{=}O + R''\bullet$	[8]
$ROO\bullet \rightarrow R' + HOO\bullet$	[9]

Our own results discussed under Task 2 also suggest the possibility of the following isomerization reaction:

$$ROO\bullet \text{---} > R'OOH + CH_2=CH\text{-}R''\bullet \qquad [10]$$

As discussed under Task 2, the FT-IR results indicate that alcohols and ketones are formed when thermally stressing the aerated fuel, which is consistent with the accepted mechanism (Reactions 1-7). It appears, however, that the alcohols decompose at high temperature (350 °C). The ketones appear to be stable at high temperature and remain soluble since the carbonyl band does not disappear with filtering. Ketone formation was observed by infrared spectroscopy in previous work at AFR (17,18,28), and more recently by Selvaraj et al. (38) and Heneghan et al. (60).

However, no alcohol formation was observed during stressing of the deaerated fuel, and the shape and position of the carbonyl band observed indicates that carboxylic acid formation occurs. This scenario is consistent with the isomerization reaction given by Reaction 10. The steady state concentration of the ROO• radical is reduced due to the lower oxygen concentration (Reaction 2), thereby prohibiting the formation of significant quantities of alcohols and ketones (Reaction 4). This results in an increased lifetime of the peroxy radical, thus allowing for carboxylic acid formation via radical isomerization (Reaction 10). Formation of carbon dioxide, which is attributed to the decomposition of carboxylic acids, was observed for both the aerated and deaerated fuels, thus suggesting that acid formation occurs in both cases. The possibility exists that acid formation results from secondary oxidation of ketones and alcohols in the presence of oxygen. However, this probability is diminished for the deaerated fuel since the oxygen concentration should be low. Carbon dioxide formation appears at lower temperature for the deaerated fuel (250 °C) and exhibits a shifted band position. With the filter on at 250 °C, the carbon dioxide band was greatly diminished. These two observations suggest that the carbon dioxide is adsorbed on the insoluble material in the deaerated fuel.

The radical isomerization reaction, [10] can be affected in two ways.

1. At approximately zero oxygen concentration, no RO_2 radicals and consequently no acid can be formed. For this purpose, the Sun fuel was very thoroughly deaerated and stressed at 350 °C. Fig. 5.3-1 shows that no acid was formed under this condition.

2. The addition of inhibitor in high enough concentrations should also decrease the acid formation if it occurred through the radical mechanism. The inhibitor used in this study was SBDTBPH. Fig. 5.3-2 shows that, in the presence of SBDTBPH, the acid formation was depressed for the partially deaerated fuel.

Modeling - One objective of the combined Phase I and Phase II program is to use the in-situ measurements of oxygenated species (alcohols, ketones, CO_2) to enhance the AFR global three step model. While our FT-IR data are consistent with the general free radical scheme outlined in equations 1-10, this mechanism is too complex for inclusion in a comprehensive fluid dynamic model (CFD) of an aircraft fuel system. Some progress toward an intermediate model has recently been made by Katta et al. (61). It is expected that time resolved measurements of oxygenated species such as alcohols, carbonyls, and CO_2 would greatly benefit model development and evaluation efforts. For example, our current model is able to predict the trends in the CO_2 formation, as shown in Fig. 5.3-3. However, the data set developed in the Phase I program is too sparse in terms of the temperature resolution (100°C) to be very useful for comparisons of this point. The transient nature of the starting fuel over the 3 month test program also introduced some variability into the measurements since the cell geometry, optical system, and test conditions have not yet been optimized. These problems will be addressed in the Phase II program.

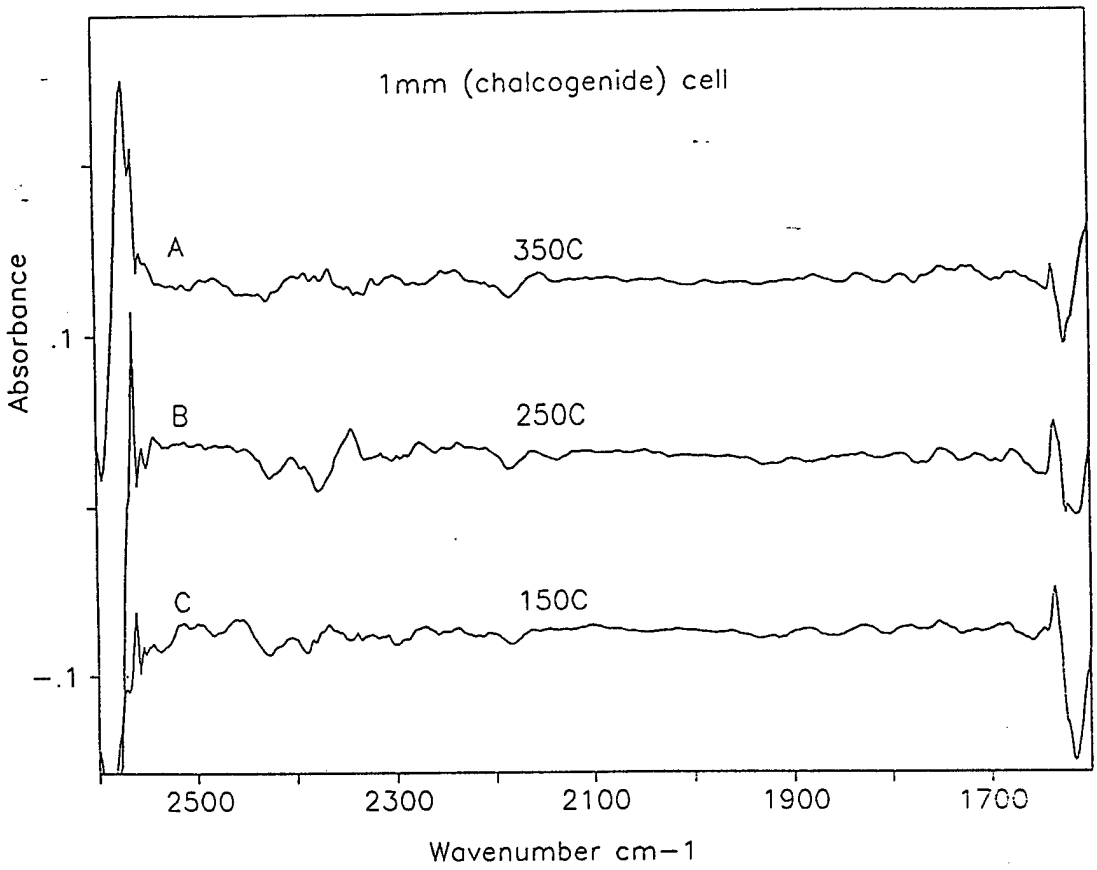

Figure 5.3-1. Spectra from Thermal Stressing of Completely Deaerated Sun Fuel Indicating Absence of Acid Formation.

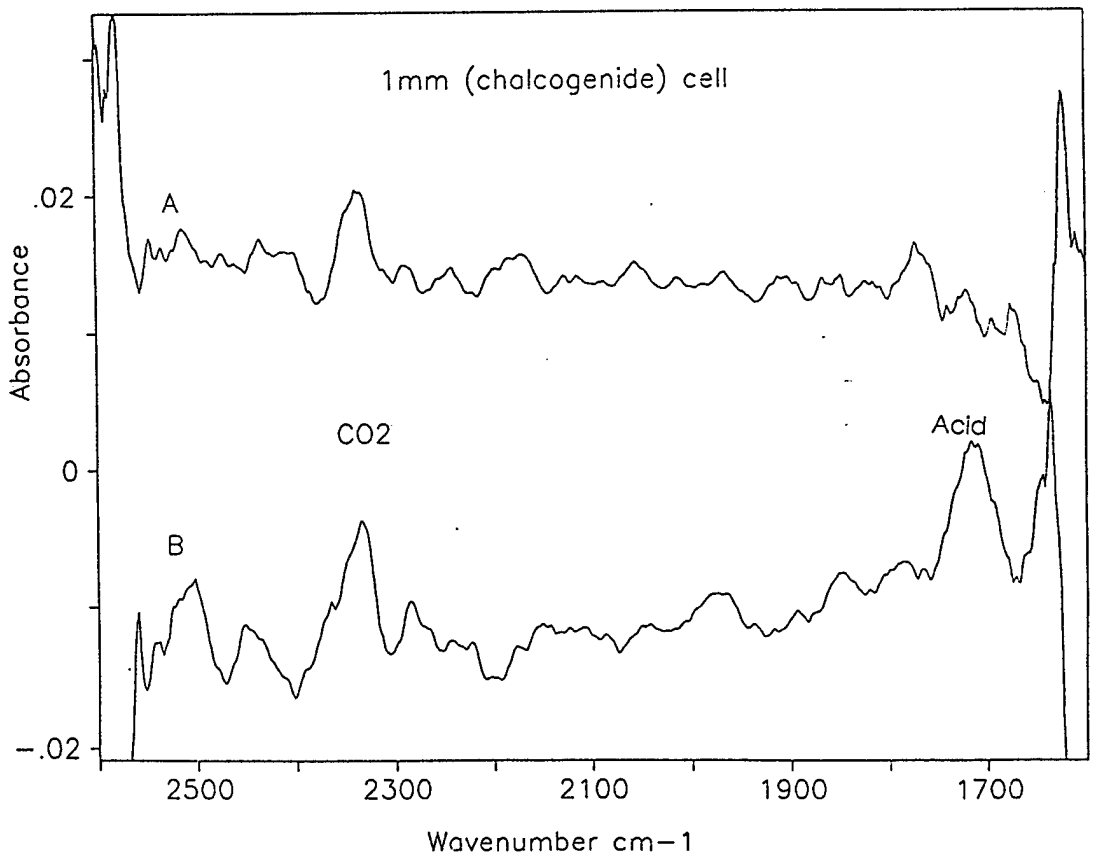

Figure 5.3-2. Spectra from Thermal Stressing of Deaerated Sun Fuel at 350°C With (a) and Without (b) Inhibitor.

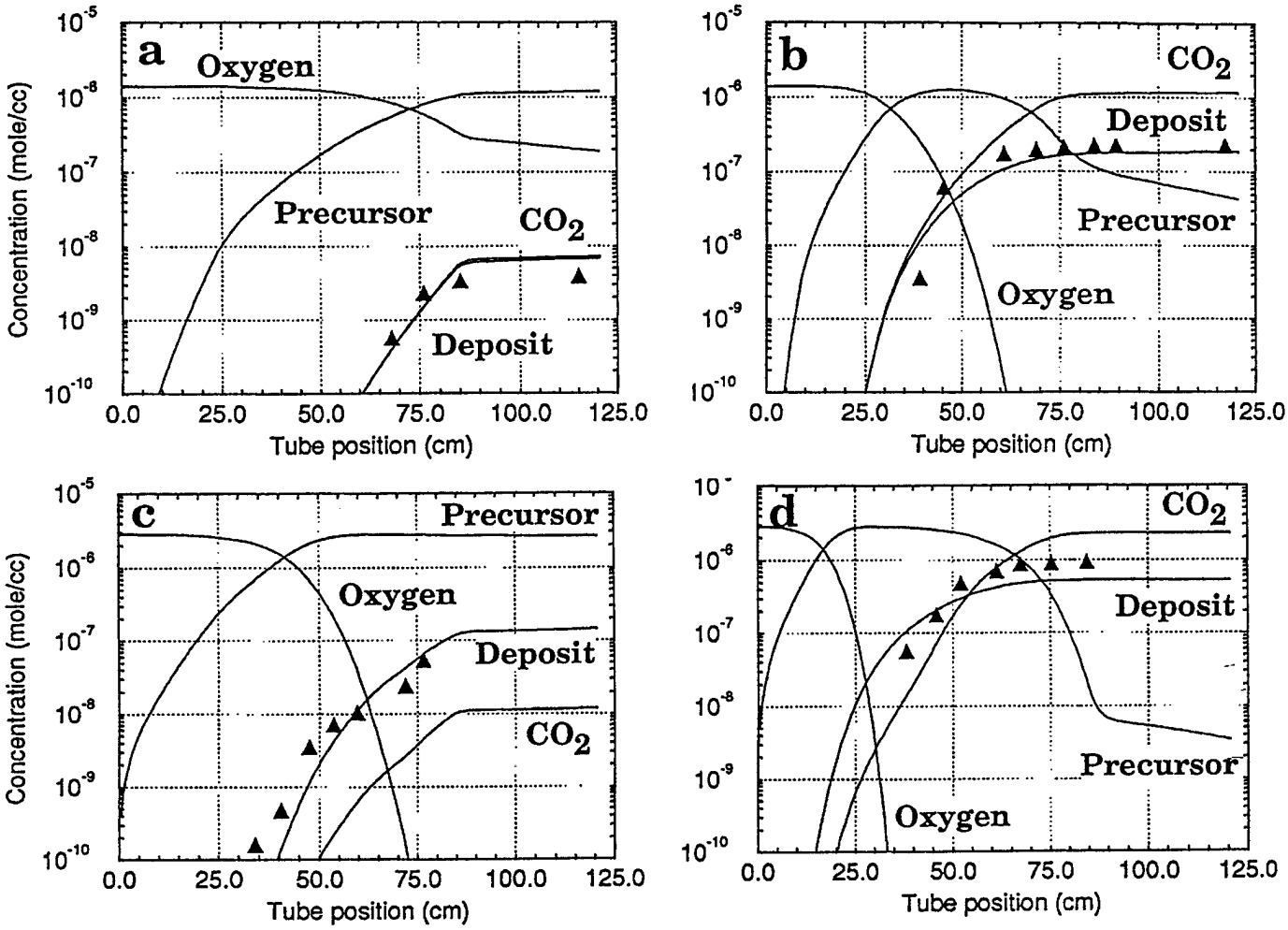

Figure 5.3-3. Comparison of AFR Model Predictions (solid lines) with Mesured Deposit Concentrations (symbols). a) Jet A - Low Temperature and Low Velocity Condition, b) Jet A - High Temperature and Low Velocity Condition, c) Suntech A - Low Temperature and d) Suntech A - High Temperature. Data from Ref. 30.

5.4. Task 4 - Investigation of On-line Raman Monitors (Option)

Objective

Assessment of FT-Raman spectroscopy as an on-line monitor for the bulk composition of stressed fuels.

Methodology

Raman Spectroscopy - Raman spectroscopy is based on the inelastic scattering of radiation by molecular oscillators (62,63). The inelastic nature of the scattering is due to the different energies (frequencies) associated with various molecular vibrations. If a sample is illuminated with a monochromatic light source, scattered light will be observed at frequencies shifted from the source radiation, and the magnitude of the shift corresponds to the frequency of the vibration. Additionally, the intensity of the scattered radiation is proportional to the concentration of the scattering species. Since the selection rules for Raman scattering are different than those for infrared absorption, Raman spectroscopy is considered to be complementary to infrared spectroscopy for chemical analysis.

Recently, advances in multiplexed spectrometers (Fourier transform) and multichannel detectors (CCD and other array detectors) have resulted in the measurement of complete spectral regions simultaneously (64,65). This has eliminated the long analysis times traditionally associated with Raman, allowing near real-time and multicomponent measurements on a continuous basis. Since Raman spectroscopy is performed in the visible or near infrared region of the spectrum, the use of highly transmittant, inexpensive communication fiber-optics has become possible (66-72).

The complementary nature of Raman spectroscopy makes this technique attractive for coupling with the FT-IR based techniques investigated in Tasks 1 and 2 of this project. Since Raman activity is based on the changing *polarizability* that is a result of molecular vibration, bands that are very weak or absent in infrared absorption spectra can often be readily observed in the Raman spectra. This is a particular advantage for vibrations involving non-polar bonds; for example, the olefin C+C stretching band is often very weak in infrared absorption spectra, but is a strong Raman scatter. Raman spectroscopy will be evaluated as a potential diagnostic technique to be included in the Advanced FSTS to be developed in Phase II, if it proves useful.

Work Performed

Much of the work was focused on analysis of samples that were collected from thermal stressing experiments done under Task 2. However, the measurements have indicated that the sensitivity of our current optical arrangement is well below that of the FT-IR transmission measurements. Figures 5.4-1a and 5.4-1b compare unstressed and mildly stressed aerated Shell fuel (500°C, 2 minutes). Within the noise level, the spectra are identical. The FT-Raman system was able to resolve differences in the C-H stetching regions between the two fuels, as can be seen by comparing Figure 5.4-2a and 5.4-2b. A second sample of Shell fuel was severely stressed (500°C, 5 hours) and the results are shown in Figs. 5.4-1c and 5.4-2c. The most obvious change is the appearance of a broad fluorescence band centered at 1500 cm^{-1}. In addition, the bands between 1020 and 1100, and the band at 1310 disappear, while the primary bands at 1450, 2871, and 2932 cm^{-1} diminish considerably. The bands at 1000 and 1385 cm^{-1} remain constant in intensity, while the bands at 1615 and 3060 cm^{-1} increase in intensity. A new band also appears at 1640 cm^{-1}. These changes are preliminarily assigned to the C=C features (1020-1100, 1450 cm^{-1}) being replaced to some degree by C-C (3060 cm^{-1}), aldehyde or ketone features (1615 and 1640 cm^{-1}). It should be noted, however, that the generation of degradation by-products required significant

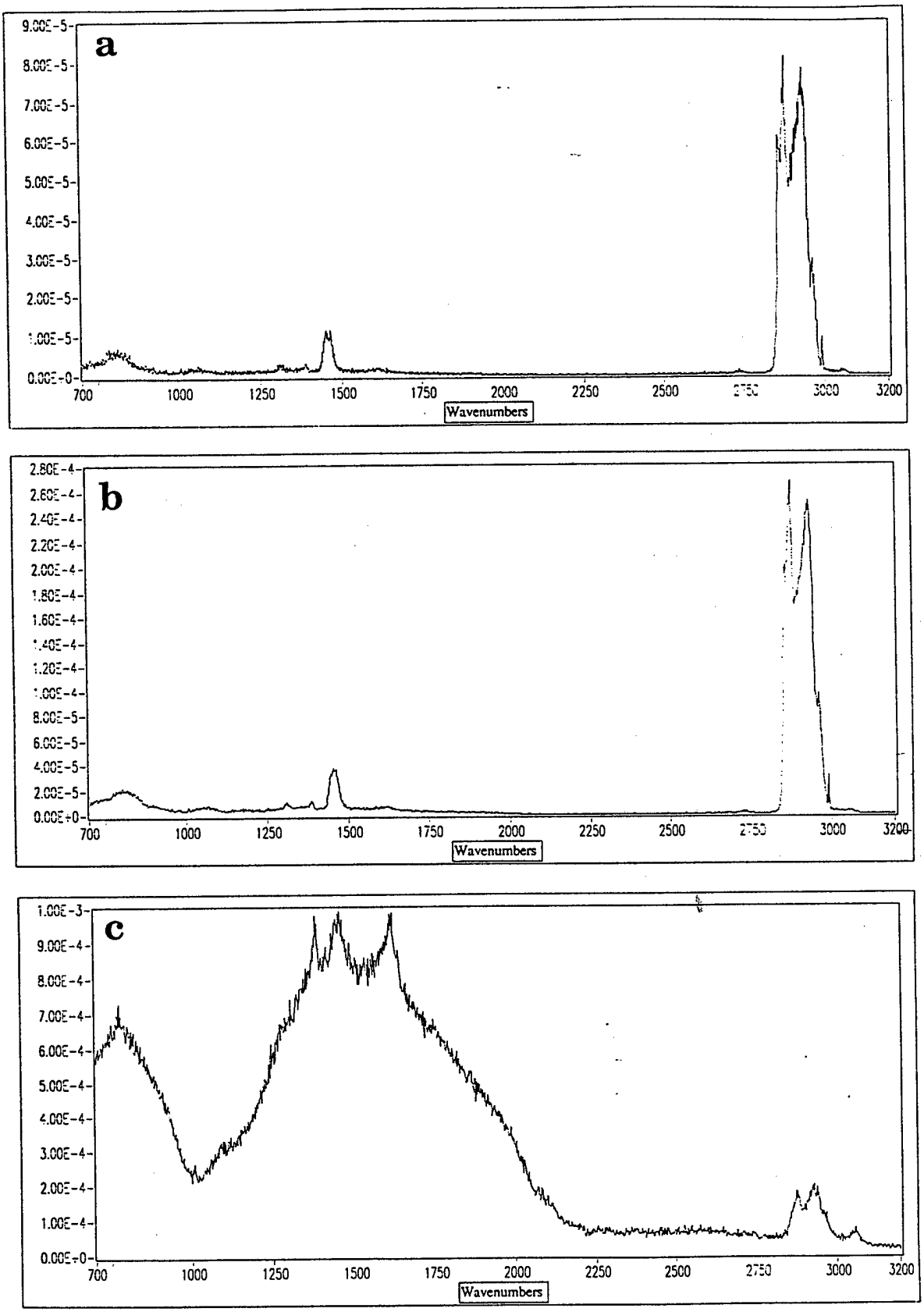

Figure 5.4-1. FT-Raman Spectra of Shell Fuel. a) Unstressed Fuel; b) Fuel Subjected to Mild Stressing at 500°C; c) Fuel Subjected to Severe Stressing at 560°C.

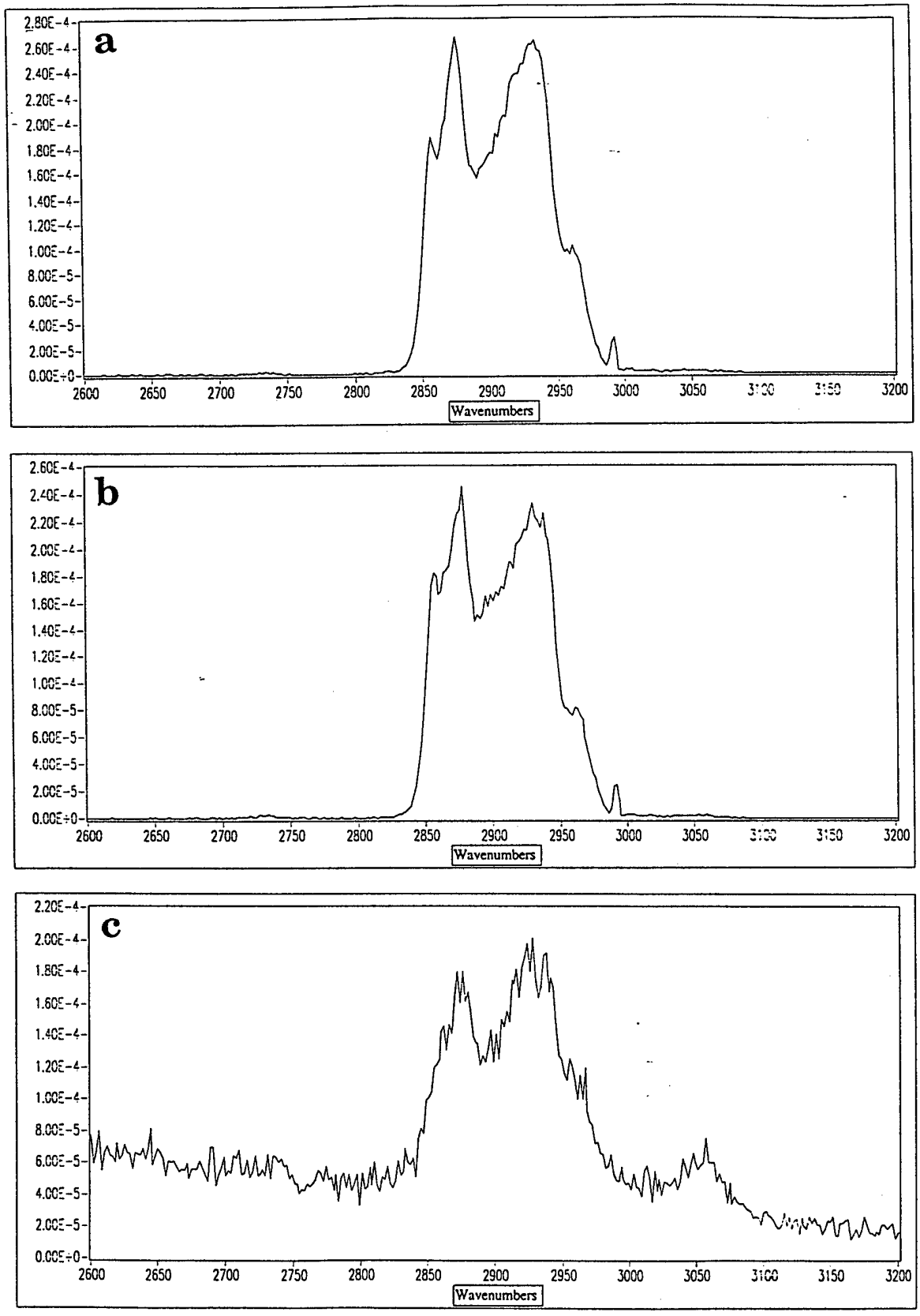

Figure 5.4-2. Comparison of C-H Stretching Regions in FT-Raman Spectra of Shell and Sun Fuels. a) Unstressed Sun Fuel; b) Unstressed Shell Fuel; c) Severely Stressed Shell Fuel.

heating, and similar spectral changes for mildly stressed fuels (as measured by infrared spectroscopy) were not observed.

The limitation in sensitivity can be overcome by surface-enhancement of the Raman signal, as discussed in Section 5.3 of the Phase II Work Plan (42).

6. CONCLUSIONS

6.1 Technical Feasibility

The Phase I program has demonstrated the feasibility of using FT-IR Fiber Optic Transmission (FOT) spectroscopy to make in-situ measurements of oxygenated species (CO_2, alcohols, carbonyls) known to be involved in fuel degradation processes and to provide reliable indications of fuel oxidative and thermal stability. The specific accomplishments of this program can be summarized as follows:

- Designed, constructed, and tested an improved Fuel Stability Test System with three high pressure in-situ fiber optic transmission cells (2 mid-infrared, 1 near-infrared)

- Designed, constructed, and tested a multiple path optical bench that could switch between the three fiber optic cells using computer controlled mirrors

- Made in-situ IR transmission measurements of peroxide decomposition products from stressed fuels including carbonyls (free and acid form), alcohols, and CO_2 (two forms). The measurements of CO_2 are believed to be the first reported measurements in a stressed jet fuel.

- Demonstrated that the IR transmission measurements are consistent with the generally accepted free radical mechanism of fuel degradation, including the inverse relationship between oxidative and thermal stability.

- Demonstrated a methodology for predicting the deposit forming tendencies by the perturbations of FT-IR transmission measurements when an in-line filter is used, which agrees well with results from the literature.

- Demonstrated that both the large gap (1 mm) and small gap (0.1 mm) IR transmission measurements were very sensitive to the presence of a steel wire probe in the quartz-lined thermal stressing reactor, which was consistent with significant changes in soluble gum formation that were also observed with the wire present.

- Completed a preliminary evaluation of FT-Raman measurements in an option task which led to the conclusion that a surface enhanced probe would be desirable to improve the sensitivity for monitoring fuel degradation.

6.2 Technical, Economical and Social Benefits

If carried through Phases II and III, this program will result in an instrument package, including software, for measurement of jet fuel thermal stability based on multiple optical methods. The program is designed to produce an instrument that will have direct application to process development activities for thermally stable fuels and supercritical fuels for hypersonic aircraft. However, the same instrument would have applications in a much wider market such as the production of gasoline which does not clog fuel injectors and the assessment of heat exchanger fouling in the petrochemical industry. A recent study at Argonne National Laboratory estimates that fouling costs a typical 100,000 barrel/day refinery ~ $14 million per year in increased energy and

maintenance costs (45). Similarly, a British study estimated the annual cost of heat exchanger surface fouling in industry as being equivalent to about 0.3% of the U.K. Gross National Product (46). The successful development of the advanced FSTS based on optical diagnostics would provide the following benefits which have commercial value: 1) A quantitative and reliable instrument for rapid measurement of fuel to thermal and oxidative stability 2) The possibility of on board monitoring of deposit buildup in aircraft engines and fuel supply systems; 3) Improved global models of fuel degradation mechanisms; 4) a knowledge base to design stable fuels or make a priori predictions of fuel stability based on composition.

6.3 Estimated Cost of Approach Relative to Benefits

The estimated cost of the combined Phase I and Phase II efforts is about $830,000. This is a relatively small amount when compared to the values of the aircraft that are being developed and the total value of the jet fuels that are used each year by the Department of Defense.

7. REFERENCES

1. Kendall, D.R. and Mills, J.S., Ind. Eng. Chem. Prod. Res. Dev., **25**, 360 (1986).
2. Hazlett, R.N., "Free Radical Reactions Related to Fuel Research," in Frontiers of Free Radical Chemistry, William A. Pyror (Ed.), Academic Press, NY, pp. 195-223 (1980).
3. Galya, L.G., Cronauer, D.C., Painter, P.C. and Li, N., Ind. Eng. Chem. Fundam., **25**, 129 (1986).
4. Zinbo, M., Jensen, R.K., Johnson, M.D. and Korak, S., Ind. Eng. Chem. Res., **26**, 902 (1987).
5. Mayo, F.R. and Lan, B.Y., Ind. Eng. Chem. Res., **26**, 215 (1987).
6. Mayo, F.R. and Lan, B.Y., Ind. Eng. Chem. Res., **25**, 333 (1986).
7. Tseregounis, S.I., Spearot, J.A. and Kite, D.J., Ind. Eng. Chem. Res., **26**, 886 (1987).
8. Leftin, H.P. and Newsome, D.S., Ind. Eng. Chem. Res., **26**, 1003 (1987).
9. Taylor, W.F., IEC Product Res. Dev., **8**, 375 (1969).
10. Busheva, E.M. and Bespolov, I.F., Khim. i Tecknol. Topliv i Masel, p. 46, Sept., 1971.
11. Sheldon, R.A. and Kochi, J.K., Metal-Catalyzed Oxidations of Organic Compounds, Academic Press, NY, (1981).
12. Naidu, S.K., Klaus, E.E., and Duda, J.L., IEC Prod. Res. Dev., **23**, 613, (1984).
13. Tevelde, J., Spadaccini, L.J., Szetela, E.J., and Glickstein, M.R., AGARD Conf. Proceedings, No. 353,
14. Marteney, P.J. and Spadaccini, L.J., Journal of Eng. For Gas Turbines and Power, **108**, 648, (1986).
15. Momenthy, A., "The Fuel Section of the NASA/Boeing Airframe Study", presented at the High Speed Commercial Transport Fuels Workshop, Oct. 14-15, 1987, NASA Lewis Research Center, Cleveland, Ohio, (1987).
16. Nixon, A.C., "A Study on Endothermic and High Energy Fuels for Airbreathing Engines", Report prepared for U.S. Air Force under Contract #F33615-84-C-2410, Battelle Columbus Div., (Jan. 22, 1986).
17. Serio, M.A., Malhotra, R., Kroo, E., Deshpande, G.V., and Solomon, P.R., "Thermal Stability of Aviation Fuels", Air Force Final Report under Contract No. F33615-88-C-2835, (March 1989).
18. Serio, M.A., Malhotra, R., Kroo, E., Deshpande, G.V., and Solomon, P.R., ACS Div. of Petr. Chem. Prepr., **34**(4), 816, (1989).
19. Deshpande, G.V., Serio, M.A., Solomon, P.R., and Malhotra, R., ACS Div. of Fuel Chem. Prepr., **34**(3), 955, (1989).
20. Rubey, W.A., Mazer, S.L., Taylor, P.H. and Stoller, J.G., ACS Pet. Div. Preprints, **32**,(2), 526 (1987).
21. Morris, R.E., and Hazlett, R.N., Energy & Fuels, **3**, 262, (1989).
22. Grigsby, R.D., Sturm, Jr., G.P., Green J.B., Goetzinger, J.W., Kamin, R.A., ACS Div. of Fuel Chem. Prepr., **34**(4), 825, (1989).
23. Roquemore, W.M., Pearce, J.A., Harrison, III, W.E., Krazinski, J.L., Vanka, S.P., ACS Div. of Fuel Chem. Prepr., **34**(4), 841, (1989).
24. Klavetter, E., Trott, W., O'Hern, T., Martin, S., "Advanced thermally Stable, Jet Fuels Development Program, Annual Report, Vol. II, Model and Experiment System Development," Final Report for Air Force WL-TR-91-2099, January (1992).
25. Parker, T.E., Foutter, R.R., Rawlins, W.T., "Optical Diagnostic Methods for the Study fo Fuel Fouling,: Ind. Eng. Chem. Res. 31, 2243-2251 (1992).
26. Striebich, R.C., Rubey, W.A., "A Condensed Phase Test Cell Assembly for the System for Thermal Diagnostic Studies (STDS), Final Rpt for Air Force WL-TR-92-2040, Aug, 1992.
27. Naegeli, D.W., Hill, R.H., "Laser Induced Fluorescence Detection of Gums in Jet Fuels," Final Report for Air Force WL-TR-92-2015, May (1992).

28. Serio, M.A., Pines, D.S., Kroo, E., Knight, K.S., Solomon, P.R., Phase I Final Report for Air Force contract No. F33615-92-C-2213 (January, 1993).
29. Serio, M.A., Pines, D.S., Kroo, E., Knight, K.S., Solomon, P.R., "In Optical Methods for Process Control, SPIE Vol. 2069, pp 20-31 (1993).
30. Giovanetti, A.J. and Szetela, E.J., "Long Term Deposit Formation in Aviation Turbine Fuel at Elevated Temperature," NASA Final Reprot, Contract No. NAS3-24091, (1985).
31. Fodor, G.E., Energy and Fuel, 2, 729, (1988).
32. Martin, S.J., Frye, G.C., Klavetter, E.A., Ricco, A.J., ACS Div. of Petr. Chem. Preprints 37, (2) 457 (1992).
33. Kamin, R.A., Mowack, C.J., and Darrah, S., Proceedings of the 3rd International Conference on Stability and Handling of Liquid Fuels. The Institute of Petroleum, London, England, 1988, Vol. 1, op. 240.
34. Heneghen, S.P., and Harrison, W.E., III, ACS Div. of Petr. Chem. Preprints, 37 (2), 404 (1992).
35. Zabarnick, S., Ind. Eng. Chem. Res., 32, 1012 (1993).
36. Edwards, T., and Zabarnick, S., Ind. Eng. Chem. Res., 32, 3117 (1993).
37. Reddy, K.T., Cernansky, N.P., and Cohen, R.J., Energy and Fuels, 2, 205, (1988).
38. Selvaraj, L., Sobkowiak, M., Coleman, M.M., ACS Div. of Petr. Chem. Prep. 37, (2) 451 (1992).
39. S.P. Heneghan, S. Zabarnick, *Fuel,* **73,** 35 (1994).
40. N.M. Emanuel, E.T. Denisov, Z.K. Maizus, *Liquid Phase Oxidation of Hydrocarbons*, Plenum Press, New York, 1967.
41. S.W. Benson, *J. Chem. Phys.*, **40**, 1007 (1964).
42. Advanced Fuel Research, Inc. Phase II SBIR proposal to Air Force, "In-Situ Methods for Study of Fuel Thermal Stability," Michael A. Serio, Principal Investigator, December 20, 1994.
43. Newman, J.S., "Principals for Fire Detection, " Fire Technology, (May 1998).
44. Heneghan, S.P., and Kauffman, 5th International Conf. on Stability and Handling of Liquid Fuels, Rotterdam (October 3-7, 1994).
45. Chemical and Engineering News, May 30, 1994, p. 16.
46. Thackery, P.A. 1979. "The Cost of Fouling in Heat Exchange Plant." Inst. Corros. Sci Tech./I. Chem. E. Conference on Fouling - Science or Art? University of Surrey, Guildford, U.K., pp. 1-9.
47. Ben-Gera, I., Norris, K.H., J. Food Sci., **33**, 64, (1968), and Isr. J. Agric. Res., **18**, 117, (1968).
48. Kelly, J.J., Callis, J.B., Anal. Chem., **62**, 1444, (1990).
49. Shah, N.K., P.J. Gemperline, *Anal. Chem.*, **62**, 465 (1990).
50. Gemperline, P.J., L.D. Webber, F.O. Cox, *Anal. Chem.*, **61**, 138 (1989).
51. Bonanno, A.S., Olinger, J.M., Griffiths, P.R., in *Near Infra-red Spectroscopy; Bridging the Gap between Data Analysis and NIR Applications*, Hildrum, Isaksson, Naes, and Tandberg, Eds., Ellis Horwood, Great Britain, 1992.
52. Bonanno, A.S., Griffiths, P.R., Short-Wave Near Infrared Spectra of Neat Organic Liquids, submitted to *J. Near Infrared Spectroscopy*, 1992.
53. Haaland, D.M., Thomas, E.V. Anal. Chem., **60**, 1193, (1988), and Anal. Chem., **60**, 1202, (1988).
54. Martens, M., Martens, H., Appl. Spectrosc., **40**, 303, (1986).
55. Brown, C.W., Obremski, R.J., Anderson, P., Appl. Spectrosc., **40**, 734, (1986).
56. Haaland, D.M., Easterling, R.G., Appl. Spectrosc., **34**, 539, (1980), and Appl. Spectrosc., **36**, 665, (1982).
57. Borello, E., Coluccia, S., and Zecchina, A., J. Catalysis, **92,** 79 (1985).
58. Solomon, P.R., Hamblen, D.G., Carangelo, R.M., Serio, M.A., and Deshpande, G.V., "A General Model of Coal Devolatilization," Energy and Fuel, **2**, 405, (1988).

59. Solomon, P.R., Hamblen, D.G., Serio, M.A., Yu, Z.Z., and Charpenay, S., Fuel **72 (4)**, 469, (1993).
60. Heneghan, S.P., Lockhear, S.L., Geiger, D.L., and Anderson, S.D., AIAA paper 90-0686, Reno, NV (January 6-9, 1992).
61. Katta, V.R., Jones, E.G., and Rocquemore, AGARD Symposium, Colleferro, Italy (May 10-14, 1993).
62. Placzek, G., UCRL Translation No. 526L from Handbuch der Radiologie, 2, (E. Marx, Ed.), Akademische Verlags Gesellschaft, Leipsag, (1934).
63. Tobias, R.S., J. Chem. Ed., **44**, 2-8, (1967).
64. Garrison, A.A., Muly, E.C., Roberts, M.J., Trimble, D.S., and Moore, C.F., ISA, Research Triangle Park, 357-363, (1989).
65. Garrison, A.A., "Optically Based Methods for Process Analysis", (D.S. Bomse, H.Brittain, S., Farquharson, J.M. Lerner, A.J. Rein, C. Sohl, T.R., Todd, and L. Weyer, Eds.,), Proc. SPIE, 1681, (1992) accepted.
66. McCreery, R.L., Fleischmann, M., and Hendra, P., Anal. Chem. ,**55**, 146-148, (1983).
67. McLachlin, R.D., Jewett, G.L., and Evans, J.C., US Patent No. 4,573,761, (1986).
68. Leugers, M.A. and McLachlan, R.D., Chemical, Biological, and Environmental Applications of Fiber, (R.A. Leiberman and M.T. Wlodarczyk, Eds.) Proc. SPIE **990**, 88-95, (1988).
69. Williamson, J.M., Bowling, R.J., and McCreery, R.L., Appl. Spectrosc., **43**, 372-375, (1989).
70. Allred, C.D. and McCreery, R.L., Appl. Spectrosc., **44**, 1229-1231, (1990).
71. Angel, S.M., Vess, T.M., and Myrick, M.L., Chemical, Biological, and Envrionmental Fiber Sensors III, (R.A. Lieberman and M.T. Wlodarczyk, Eds.), Proc. SPIE, **1587**, 219-231, (1991).
72. Carrabba, M.M. Spenser, K.M., and Rauh, R.D., in Environmental Sensing and Combustion Diagnostics, (J.J. Santoleri, Ed.), Proc. SPIE, **1434**, 127-134, (1991).